Rate of quantum ergodicity in Euclidean billiards

A. Bäcker* and R. Schubert†
Abteilung Theoretische Physik, Universität Ulm, 89069 Ulm, Federal Republic of Germany

P. Stifter‡
Abteilung Quantenphysik, Universität Ulm, 89069 Ulm, Federal Republic of Germany
(Received 9 October 1997; revised manuscript received 15 January 1998)

For a large class of quantized ergodic flows the quantum ergodicity theorem states that almost all eigenfunctions become equidistributed in the semiclassical limit. In this work we give a short introduction to the formulation of the quantum ergodicity theorem for general observables in terms of pseudodifferential operators and show that it is equivalent to the semiclassical eigenfunction hypothesis for the Wigner function in the case of ergodic systems. Of great importance is the rate by which the quantum-mechanical expectation values of an observable tend to their mean value. This is studied numerically for three Euclidean billiards (stadium, cosine, and cardioid billiard) using up to 6000 eigenfunctions. We find that in configuration space the rate of quantum ergodicity is strongly influenced by localized eigenfunctions such as bouncing-ball modes or scarred eigenfunctions. We give a detailed discussion and explanation of these effects using a simple but powerful model. For the rate of quantum ergodicity in momentum space we observe a slower decay. We also study the suitably normalized fluctuations of the expectation values around their mean and find good agreement with a Gaussian distribution. [S1063-651X(98)13305-6]

PACS number(s): 05.45.+b, 03.65.−w, 03.65.Ge

I. INTRODUCTION

In quantum chaos much work is devoted to the investigation of the statistics of eigenvalues and properties of eigenfunctions of quantum systems whose classical counterpart is chaotic. For ergodic systems the behavior of almost all eigenfunctions in the semiclassical limit is described by the quantum ergodicity theorem, which was proved in [1–5]; see also [6,7] for general introductions. Roughly speaking, it states that for almost all eigenfunctions the expectation values of a certain class of quantum observables tend to the mean value of the corresponding classical observable in the semiclassical limit.

Another commonly used description of a quantum-mechanical state is the Wigner function [8], which is a phase-space representation of the wave function. According to the ''semiclassical eigenfunction hypothesis,'' the Wigner function concentrates in the semiclassical limit on regions in phase space that a generic orbit explores in the long-time limit $t\to\infty$ [9–12]. For integrable systems the Wigner function $W(p,q)$ is expected to localize on the invariant tori, whereas for ergodic systems the Wigner function should semiclassically condense on the energy surface, i.e., $W(p,q)\sim[1/V(\Sigma_E)]\delta(H(p,q)-E)$, where $H(p,q)$ is the Hamilton function and $V(\Sigma_E)$ is the volume of the energy shell defined by $H(p,q)=E$.

As we will show below, the quantum ergodicity theorem is equivalent to the validity of the semiclassical eigenfunction hypothesis for almost all eigenfunctions if the classical system is ergodic. Thus a weak form of the semiclassical eigenfunction hypothesis is proved for ergodic systems.

For practical purposes it is important to know not only the semiclassical limit of expectation values or Wigner functions, but also how fast this limit is achieved, because in applications one usually has to deal with finite values of $\hbar$ or finite energies, respectively. Thus the so-called rate of quantum ergodicity determines the practical applicability of the quantum ergodicity theorem. A number of articles have been devoted to this subject; see, e.g., [13–15,6,16] and references therein. The principal aim of this paper is to investigate the rate of quantum ergodicity numerically for different Euclidean billiards and to compare the results with the existing analytical results and conjectures. A detailed numerical analysis of the rate of quantum ergodicity for hyperbolic surfaces and billiards can be found in [17].

Two problems arise when one wants to study the rate of quantum ergodicity numerically. First, the fluctuations of the expectation values around their mean can be so large that it is hard or even impossible to infer a decay rate. This problem can be overcome by studying the cumulative fluctuations

$$S_1(E,A)=\frac{1}{N(E)}\sum_{E_n\leqslant E}\left|\langle\psi_n,A\psi_n\rangle-\overline{\sigma(A)}\right|, \qquad (1)$$

where $\langle\psi_n,A\psi_n\rangle$ is the expectation value of the quantum observable A, $\overline{\sigma(A)}$ is the mean value of the corresponding classical observable $\sigma(A)$, and $N(E)$ is the spectral staircase function; see Sec. II for detailed definitions. So $S_1(E,A)$ contains all information about the rate by which the quantum expectation values tend to the mean value, but is a much smoother quantity than the sequence of differences itself.

Second, since the quantum ergodicity theorem makes only a statement about almost all eigenfunctions (i.e., a subsequence of density one; see below), there is the possibility of non-quantum-ergodic subsequences of eigenfunctions. Such

*Electronic address: baec@physik.uni-ulm.de
†Electronic address: schub@physik.uni-ulm.de
‡Electronic address: stif@physik.uni-ulm.de

eigenfunctions can be, for example, so-called scarred eigenfunctions [18,19], which are localized around unstable periodic orbits, or in billiards with two parallel walls, so-called bouncing-ball modes, which are localized on the family of bouncing-ball orbits.

Although such subsequences of exceptional eigenfunctions are of density zero, they may have a considerable influence on the behavior of $S_1(E,A)$. This is what we find in our numerical computations for the cosine, stadium, and cardioid billiards, which are based on 2000 eigenfunctions for the cosine billiard and up to 6000 eigenfunctions for the stadium and cardioid billiard.

In order to obtain a quantitative understanding of the influence of non-quantum-ergodic subsequences on the rate, we develop a simple model for $S_1(E,A)$ that is tested for the corresponding billiards. The application of this model in the case of the stadium billiard reveals, in addition to the bouncing-ball modes, a subsequence of eigenfunctions, which appear to be non-quantum-ergodic in the considered energy range.

A further interesting question is if the boundary conditions have any influence on the rate of quantum ergodicity. This is indeed the case. For observables located near the boundary a strong influence on the behavior of $S_1(E,A)$ is observed. However, for $E\to\infty$ this influence vanishes, so the asymptotic rate is independent of the boundary conditions.

After having some knowledge of the rate by which the expectation values $\langle\psi_n,A\psi_n\rangle$ tend to their quantum-ergodic limit $\overline{\sigma(A)}$, one is interested in how the suitably normalized fluctuations $\langle\psi_n,A\psi_n\rangle-\overline{\sigma(A)}$ are distributed. It is conjectured that they obey a Gaussian distribution, which we can confirm from our numerical data.

The outline of the paper is as follows. In Sec. II we first give a short introduction to the quantum ergodicity theorem and its implications. Then we discuss conjectures and theoretical arguments for the rate of quantum ergodicity given in the literature. In particular we study the influence of non-quantum-ergodic eigenfunctions. In Sec. III we give a detailed numerical study on the rate of quantum ergodicity for three Euclidean billiard systems for different types of observables, both in position and in momentum space. This includes a study of the influence of the boundary and a study of the fluctuations of the normalized expectation values around their mean. We conclude with a summary. Some of the more technical considerations using pseudodifferential operators are given in the Appendixes.

II. QUANTUM ERGODICITY

The classical systems under consideration are given by the free motion of a point particle inside a compact two-dimensional Euclidean domain $\Omega\subset\mathbf{R}^2$ with a piecewise smooth boundary, where the particle is elastically reflected. The phase space is given by $\mathbf{R}^2\times\Omega$ and the Hamilton function is (in units $2m=1$)

$$H(p,q)=p^2. \tag{2}$$

The trajectories of the flow generated by $H(p,q)$ lie on surfaces of constant energy E,

$$\Sigma_E:=\{(p,q)\in\mathbf{R}^2\times\Omega\,|\,p^2=E\}, \tag{3}$$

which obey the scaling property $\Sigma_E=E^{1/2}\Sigma_1$ $:=\{(E^{1/2}p,q)\,|\,(p,q)\in\Sigma_1\}$ since the Hamilton function is quadratic in p. Note that Σ_1 is just $S^1\times\Omega$.

The classical observables are functions on phase space $\mathbf{R}^2\times\Omega$ and the mean value of an observable $a(p,q)$ at energy E is given by

$$\overline{a^E}=\frac{1}{V(\Sigma_E)}\int_{\Sigma_E}a(p,q)\,d\mu$$
$$=\frac{1}{V(\Sigma_E)}\int\int_{\mathbf{R}^2\times\Omega}a(p,q)\,\delta(p^2-E)\,dp\,dq, \tag{4}$$

where $d\mu=\frac{1}{2}d\varphi\,dq$ is the Liouville measure on Σ_E and $V(\Sigma_E)=\int_{\Sigma_E}d\mu$. The unusual factor 1/2 in the Liouville measure is due to the fact that we have chosen p^2 and not $p^2/2$ as the Hamilton function. For the mean value at energy $E=1$ we will for simplicity write $\overline{a}$.

The corresponding quantum system that we will study is given by the Schrödinger equation (in units $\hbar=2m=1$)

$$-\Delta\psi_n(q)=E_n\psi_n(q),\quad q\in\Omega, \tag{5}$$

with Dirichlet boundary conditions $\psi_n(q)=0$ for $q\in\partial\Omega$. Here $\Delta=\partial^2/\partial q_1^2+\partial^2/\partial q_2^2$ denotes the usual Laplacian and we will assume that the eigenvalues are ordered as $E_1\leqslant E_2\leqslant E_3\cdots$ and that the eigenfunctions are normalized $\int_\Omega|\psi_n(q)|^2dq=1$.

The quantum ergodicity theorem describes the behavior of expectation values $\langle\psi_n,A\psi_n\rangle$ in the high-energy (semiclassical) limit $E_n\to\infty$ and relates it to the classical mean value (4). The observable A is assumed to be a pseudodifferential operator, so before we state the theorem we have to introduce the concept of pseudodifferential operators; see, e.g., [20–23].

A. Weyl quantization and pseudodifferential operators

It is well known that every continuous operator $A:C_0^\infty(\Omega)\to\mathcal{D}'(\Omega)$ is characterized by its Schwarz kernel $K_A\in\mathcal{D}'(\Omega\times\Omega)$ such that $A\psi(q)=\int_\Omega K_A(q,q')\psi(q')dq'$, where $\mathcal{D}'(\Omega)$ is the space of distributions dual to $C_0^\infty(\Omega)$; see, e.g., [24], Chap. 5.2. In Dirac notation one has $K_A(q,q')=\langle q|A|q'\rangle$. With such an operator A one can associate its Weyl symbol, defined as

$$W[A](p,q):=\int_{\mathbf{R}^2}e^{iq'p}K_A\left(q-\frac{q'}{2},q+\frac{q'}{2}\right)dq', \tag{6}$$

which in general is a distribution [21]. An operator A is called a pseudodifferential operator if its Weyl symbol belongs to a certain class of functions. One of the simplest classes of symbols is $S^m(\mathbf{R}^2\times\Omega)$, which is defined as follows: $a(p,q)\in S^m(\mathbf{R}^2\times\Omega)$ if it is in $C^\infty(\mathbf{R}^2\times\Omega)$ and for all multiple indices α,β the estimate

$$\left|\frac{\partial^{|\alpha|}}{\partial p^\alpha}\frac{\partial^{|\beta|}}{\partial q^\beta}a(p,q)\right|\leqslant C_{\alpha,\beta}(1+|p|^2)^{(m-|\alpha|)/2} \tag{7}$$

holds. Here m is called the order of the symbol. The main point in this definition is that differentiation with respect to p

lowers the order of the symbol. For instance, polynomials of degree m in p, $\Sigma_{|\alpha'|\leq m} c_{\alpha'}(q)p^{\alpha'}$, whose coefficients satisfy $|(\partial^{|\beta|}/\partial q^{\beta})c_{\alpha'}(q)| \leq C_{\alpha',\beta}$, are in $S^m(\mathbf{R}^2\times\Omega)$.

An operator A is called a pseudodifferential operator of order m, $A\in S^m(\Omega)$, if its Weyl symbol belongs to the symbol class $S^m(\mathbf{R}^2\times\Omega)$,

$$A\in S^m(\Omega) :\Leftrightarrow W[A](p,q)\in S^m(\mathbf{R}^2\times\Omega). \tag{8}$$

For example, if the Weyl symbol is a polynomial in p, then the operator is in fact a differential operator and so pseudodifferential operators are generalizations of differential operators. Further examples include complex powers of the Laplacian $(-\Delta)^{z/2}\in S^{\Re z}(\Omega)$; see [25,26,22].

On the other hand, with any function $a\in S^m(\mathbf{R}^n\times\Omega)$ one can associate an operator $\hat{a}\in S^m(\Omega)$,

$$\hat{a}f(q) := \frac{1}{(2\pi)^2}\int\int_{\Omega\times\mathbf{R}^n} e^{i(q-q')p} a\left(p,\frac{q+q'}{2}\right) \times f(q')dq'dp, \tag{9}$$

such that its Weyl symbol is a, i.e., $W[\hat{a}]=a$. This association of the symbol a with the operator $\hat{a}$ is called Weyl quantization of a.

In practice one often encounters symbols with a special structure, namely, those that have an asymptotic expansion in homogeneous functions in p,

$$a(p,q)\sim\sum_{k=0}^{\infty} a_{m-k}(p,q)$$

with

$$a_{m-k}(\lambda p,q)=\lambda^{m-k}a_{m-k}(p,q) \quad \text{for } \lambda>0. \tag{10}$$

Note that it is not required that m be an integer; all $m\in\mathbf{R}$ are allowed. Since the degree of homogeneity tends to $-\infty$, this can be seen as an expansion for $|p|\to\infty$; see [20,21] for the exact definition of this asymptotic series. These symbols are often called classical or polyhomogeneous and we will consider only operators with Weyl symbols of this type. The space of these operators will be denoted by $S^m_{\mathrm{cl}}(\Omega)$. If $A\in S^m_{\mathrm{cl}}(\Omega)$ and $W(A)\sim\Sigma_{k=0}^{\infty}a_{m-k}$, then the leading term $a_m(p,q)$ is called the principal symbol of A and is denoted by $\sigma(A)(p,q) := a_m(p,q)$. It plays a distinguished role in the theory of pseudodifferential operators. One reason for this is that operations such as multiplication or taking the commutator are rather complicated in terms of the symbol, but simple for the principal symbol. For instance, one has [20,21]

$$\sigma(AB)=\sigma(A)\sigma(B), \quad \sigma([A,B])=i\{\sigma(A),\sigma(B)\}, \tag{11}$$

where $\{,\}$ is the Poisson bracket. It furthermore turns out that the principal symbol is a function on phase space, i.e., it has the right transformation properties under coordinate transformations, whereas the full Weyl symbol does not have this property.

So every operator A with principal symbol $\sigma(A)$ can be seen as a quantization of the classical observable $\sigma(A)$. The existence of different operators with the same principal symbol just reflects the fact that the quantization process is not unique. Furthermore, one can show that the leading asymptotic behavior of expectation values of such operators for high energies only depends on the principal symbol, as it should be according to the correspondence principle. This is a special case of the Szegö limit theorem; see [27], Chap. 29.1.

One advantage of the Weyl quantization over other quantization procedures is that the Wigner function of a state $|\psi\rangle$ appears naturally as the Weyl symbol of the corresponding projection operator $|\psi\rangle\langle\psi|$,

$$W[|\psi\rangle\langle\psi|](p,q)=\int_{\mathbf{R}^2} e^{iq'p}\overline{\psi}\left(q-\frac{q'}{2}\right)\psi\left(q+\frac{q'}{2}\right)dq'. \tag{12}$$

In the following we will use for a Wigner function of an eigenstate ψ_n the simpler notation $W_n(p,q) := W[|\psi_n\rangle\langle\psi_n|](p,q)$. For the expectation value $\langle\psi,A\psi\rangle$ one has the well-known expression in terms of the Weyl symbol $W[A]$ and the Wigner function $W[|\psi\rangle\langle\psi|]$,

$$\langle\psi,A\psi\rangle=\frac{1}{(2\pi)^2}\int\int_{\Omega\times\mathbf{R}^2} W[A](p,q)W[|\psi\rangle\langle\psi|](p,q) \times dp\,dq. \tag{13}$$

Pseudodifferential operators of order zero have a bounded Wigner function and therefore a bounded principal symbol $\sigma(A)$; this boundedness of the classical observable carries over to the operator level: The operators in $S^0(\Omega)$ are bounded in the L^2 norm.

The definition of pseudodifferential operators can be generalized to manifolds of arbitrary dimension; the previous formulas are then valid in local coordinates. The symbols of these operators exist only in local charts, but the principal symbols can be glued together to a function on the cotangent bundle $T^*\Omega$, which is the classical phase space. (If one wants to realize the semiclassical limit not as the high-energy limit but as the limit of $\hbar\to 0$, one has to incorporate $\hbar$ explicitly in the quantization procedure. In the framework of pseudodifferential operators this has been done by Voros in [9,10]; see also [28,7].)

B. Quantum limits and the quantum ergodicity theorem

In quantum mechanics the states are elements of a Hilbert space or, more generally, linear functionals on the algebra of observables. In classical mechanics the pure states are points in phase space and the observables are functions on phase space. More generally, the states are measures on phase space, which are linear functionals on the algebra of observables. The pure states are then represented as δ functions. The eigenstates of a Hamilton operator are those that are invariant under the time evolution defined by H. In the semiclassical limit they should somehow converge to measures on phase space that are invariant under the classical Hamiltonian flow. The measures that can be obtained as semiclassical limits of quantum eigenstates are called quantum limits.

More concretely, the quantum limits can be described as limits of sequences of Wigner functions. Let $\{\psi_n\}_{n\in\mathbf{N}}$ be an orthonormal basis of eigenfunctions of the Dirichlet Laplac-

ian $-\Delta$ and $\{W_n\}_{n\in\mathbf{N}}$ the corresponding set of Wigner functions; see Eq. (12). We first consider expectation values for operators of order zero and then extend the results to operators of arbitrary order.

Because pseudodifferential operators of order zero are bounded, the sequence of expectation values $\{\langle\psi_n,A\psi_n\rangle\}_{n\in\mathbf{N}}$ is bounded too. Every function $a\in C^\infty(\Sigma_1)$ can be extended to a function in $C^\infty(\mathbf{R}^2\backslash\{0\}\times\Omega)$ by requiring it to be homogeneous of degree zero in p. Via the quantization $\hat{a}$ of a and Eq. (13), one can view the Wigner function $W_n(p,q)$ as a distribution on $C^\infty(\Sigma_1)$,

$$a\mapsto\langle\psi_n,\hat{a}\psi_n\rangle=\frac{1}{(2\pi)^2}\int\int_{\Omega\times\mathbf{R}^2}a(p,q)\times W_n(p,q)dp\,dq. \tag{14}$$

(Strictly speaking, a is not an allowed symbol because it is not smooth at $p=0$. Let $\chi(p)\in C^\infty(\mathbf{R}^2)$ satisfy $\chi(p)=0$ for $|p|\leqslant 1/4$ and $\chi(p)=1$ for $|p|\geqslant 1/2$. By multiplying a with this excision function $\chi(p)$ we get a symbol $\chi a\in S^0(\mathbf{R}^2\times\Omega)$, whose Weyl quantization $\widehat{\chi a}$ is in $S^0(\Omega)$. However, the semiclassical properties of $\widehat{\chi a}$ are independent of the special choice of $\chi(p)$, which can be seen, e.g., in Eq. (14), since W_n is concentrated on the energy shell Σ_{E_n} for $n\to\infty$. Therefore, we will proceed for simplicity with a instead of χa.) The sequence of these distributions is bounded because the operators $\hat{a}$ are bounded. The accumulation points of $\{W_n(p,q)\}_{n\in\mathbf{N}}$ are called quantum limits $\mu_k(p,q)$ and we label them by $k\in I$, where I is some index set. Corresponding to the accumulation points $\mu_k(p,q)$, the sequence $\{W_n(p,q)\}_{n\in\mathbf{N}}$ can be split into disjoint convergent subsequences $\cup_{k\in I}\{W_{n_j^k}(p,q)\}_{j\in\mathbf{N}}=\{W_n(p,q)\}_{n\in\mathbf{N}}$. That is, for every k we have

$$\lim_{j\to\infty}\int\int_{\Omega\times\mathbf{R}^2}a(p,q)W_{n_j^k}(p,q)dp\,dq=\int\int_{\Omega\times\mathbf{R}^2}a(p,q)\mu_k(p,q)dp\,dq \tag{15}$$

for all $a\in C^\infty(\Sigma_1)$ viewed as homogeneous functions of degree zero on phase space. This splitting is unique up to a finite number of terms, in the sense that for two different splittings the subsequences belonging to the same accumulation point differ only by a finite number of terms. As has been shown in [29], the quantum limits μ_k are measures on Σ_1 that are invariant under the classical flow generated by $H(p,q)$.

One of the main questions in the field of quantum chaos is which classical invariant measures on Σ_1 can actually occur as quantum limits of Wigner functions. For example, if the orbital measure along an unstable periodic orbit occurs as quantum limit μ_k, then the corresponding subsequence of eigenfunctions has to show an enhanced probability, i.e., scarring, along that orbit.

Given any quantum limit μ_k, one is furthermore interested in the counting function $N_k(E):=\#\{E_{n_j^k}\leqslant E\}$ for the corresponding subsequence $\{W_{n_j^k}\}_{j\in\mathbf{N}}$ of Wigner functions. Since the subsequence $\{W_{n_j^k}\}_{j\in\mathbf{N}}$ is unique up to a finite number of elements, the corresponding counting function $N_k(E)$ is unique up to a constant.

One should keep in mind that we have defined the quantum limits and their counting functions here with respect to one chosen orthonormal basis of eigenfunctions $\{\psi_n(q)\}_{n\in\mathbf{N}}$. If one takes a different orthonormal base of eigenfunctions $\{\widetilde{\psi}_n(q)\}_{n\in\mathbf{N}}$, the counting functions corresponding to the quantum limits, or even the quantum limits themselves, may change. So when studying the set of all quantum limits, one has to take all bases of eigenfunctions into account.

The lift of any quantum limit from Σ_1 to the whole phase space $\mathbf{R}^2\times\Omega$ follows straight-forwardily from some well-known methods in pseudodifferential operator theory, as shown in Appendix B. For a pseudodifferential operator of order m, $A\in S^m_{\mathrm{cl}}(\Omega)$, one gets for the expectation values

$$\lim_{j\to\infty}E_{n_j^k}^{-m/2}\langle\psi_{n_j^k},A\psi_{n_j^k}\rangle=\mu_k(\sigma(A)|_{\Sigma_1})=\int_{\Sigma_1}\sigma(A)(p,q)\mu_k(p,q)d\mu. \tag{16}$$

In terms of the Wigner functions this expression can be written as (see Appendix C)

$$\lim_{j\to\infty}E_{n_j^k}^{n/2}W_{n_j^k}(E_{n_j^k}^{1/2}p,q)=\mu_k(p,q)\frac{\delta(H(p,q)-1)}{V(\Sigma_1)}. \tag{17}$$

Without the scaling of p with $\sqrt{E}$ we have

$$W_{n_j^k}(p,q)\sim\mu_k(p,q)\frac{\delta(H(p,q)-E_{n_j^k})}{V(\Sigma_{E_{n_j^k}})} \tag{18}$$

for $E_{n_j^k}\longrightarrow\infty$ and $\mu_k(p,q)$ is extended from Σ_1 to the whole phase space by requiring it to be homogeneous of degree zero in p.

For ergodic systems the only invariant measure whose support has nonzero Liouville measure is the Liouville measure itself. For these systems the quantum ergodicity theorem states that almost all eigenfunctions have the Liouville measure as quantum limit.

Quantum ergodicity theorem [30]. Let $\Omega\subset\mathbf{R}^2$ be a compact two-dimensional domain with piecewise smooth boundary and let $\{\psi_n\}$ be an orthonormal set of eigenfunctions of the Dirichlet Laplacian Δ on Ω. If the classical billiard flow on the energy shell $\Sigma_1=S^1\times\mathbf{R}^2$ is ergodic, then there is a subsequence $\{n_j\}\subset\mathbf{N}$ of density one such that

$$\lim_{j\to\infty}\langle\psi_{n_j},A\psi_{n_j}\rangle=\overline{\sigma(A)} \tag{19}$$

for every polyhomogeneous pseudodifferential operator $A\in S^0(\Omega)$ of order zero, whose Schwarz kernel $K_A(q,q')=\langle q|A|q'\rangle$ has support in the interior of $\Omega\times\Omega$. Here $\sigma(A)$ is the principal symbol of A and $\overline{\sigma(A)}$ is its classical expectation value; see Eq. (4).

A subsequence $\{n_j\}\subset\mathbf{N}$ has density one if

$$\lim_{E\to\infty}\frac{\#\{n_j|E_{n_j}<E\}}{N(E)}=1, \tag{20}$$

where $N(E):=\#\{n|E_n<E\}$ is the spectral staircase function, counting the number of energy levels below a given energy E. So almost all expectation values of a quantum observable tend to the mean value of the corresponding classical observable.

The special situation that there is only one quantum limit, i.e., the Liouville measure, is called unique quantum ergodicity. This behavior is conjectured to be true for the eigenfunctions of the Laplacian on a compact manifold of negative curvature [6,15].

We have stated here for simplicity the quantum ergodicity theorem only for two-dimensional Euclidean domains, but it is true in far more general situations. For compact Riemannian manifolds without a boundary the quantum ergodicity theorem was given by Shnirelman [1], Zelditch [3], and Colin de Verdière [4]. For a certain class of manifolds with a boundary it was proved in [31], without the restriction on the support of the Schwarz kernel of the operator A. The techniques of [31] can possibly be used to remove these restrictions here as well; see the remarks in [30]. One can allow as well more general Hamilton operators; on manifolds without a boundary every elliptic self-adjoint operator in $S^2_{\mathrm{cl}}(\Omega)$ is allowed and on manifolds with a boundary at least every second-order elliptic self-adjoint differential operator with smooth coefficients is allowed. This includes, for instance, a free particle in a smooth potential or in a magnetic field. In the semiclassical setting, where the Hamilton operator and the observables depend explicitly on $\hbar$, a similar theorem for the limit $\hbar\to 0$ has been proved in [5]; see also [7] for an introduction.

In light of the correspondence principle, the quantum ergodicity theorem appears very natural: Classical ergodicity means that for a particle moving along a generic trajectory with energy E, the probability of finding it in a certain region $U\subset\Sigma_E$ of phase space is proportional to the volume $V(U)$ of that region, but does not depend on the shape or location of U. The corresponding quantum observable is the quantization of the characteristic function χ_U of U and by the correspondence principle one expects that the expectation value of this observable in the state ψ_n tends to the classical expectation value for $E_n\to\infty$. This is the content of the quantum ergodicity theorem.

In terms of the Wigner functions W_n the theorem gives [see Eq. (18)]

$$W_{n_j}(p,q)\sim\frac{\delta(H(p,q)-E_{n_j})}{V(\Sigma_{E_{n_j}})} \tag{21}$$

for $j\to\infty$, for a subsequence $\{n_j\}\subset\mathbf{N}$ of density one. So almost all Wigner functions become equidistributed on the energy shells $\Sigma_{E_{n_j}}$. That is, for ergodic systems the validity of the semiclassical eigenfunction hypothesis for a subsequence of density one is equivalent to the quantum ergodicity theorem.

C. Examples

As an illustration of the quantum ergodicity theorem and for later use, we now consider some special observables whose symbol only depends on the position q or on the momentum p. If the symbol depends only on the position q, i.e., $a(p,q)=a(q)$, the operator is just the multiplication operator with the function $a(q)$ and one has

$$\langle\psi,\mathrm{A}\psi\rangle=\langle\psi,a\psi\rangle=\int_\Omega a(q)|\psi(q)|^2dq. \tag{22}$$

In the special case that one wants to measure the probability of the particle to be in a given domain $D\subset\Omega$, the symbol is the characteristic function of D, i.e., $a(p,q)=\chi_D(q)$. Then $\hat{\chi}_D$ is not a pseudodifferential operator, but nevertheless the quantum ergodicity theorem remains valid for this observable [4]. Since the principal symbol is then $\sigma(\mathrm{A})=\chi_D$, we obtain for its mean value

$$\overline{\sigma(\mathrm{A})}=\frac{1}{V(\Sigma_1)}\int_{S^1\times\Omega}\chi_D(q)d\mu=\frac{V(D)}{V(\Omega)}. \tag{23}$$

Thus the quantum ergodicity theorem gives for this case

$$\lim_{j\to\infty}\int_D|\psi_{n_j}(q)|^2dq=\frac{V(D)}{V(\Omega)} \tag{24}$$

for a subsequence $\{n_j\}\subset\mathbf{N}$ of density one. As discussed at the end of Sec. II B, this is what one should expect from the correspondence principle.

If instead the symbol depends only on the momentum p, i.e., $a(p,q)=a(p)$, one obtains from Eq. (13) for the expectation value

$$\langle\psi,\mathrm{A}\psi\rangle=\int_{\mathbf{R}^2}a(p)|\hat{\psi}(p)|^2dp. \tag{25}$$

In the same way as in [4] for a characteristic function in position space, it follows that the quantum ergodicity theorem remains valid for the case where $a(p)=\chi_{C(\theta,\Delta\theta)}(p)$ is the characteristic function of a circular sector in momentum space of angle θ. In polar coordinates this is given by the set

$$C(\theta,\Delta\theta):=\{(r,\varphi)|r\in\mathbf{R}^+,\varphi\in[\theta-\Delta\theta/2,\theta+\Delta\theta/2]\}. \tag{26}$$

The mean value of the principal symbol then reduces to

$$\overline{\sigma(\mathrm{A})}=\frac{1}{V(\Sigma_1)}\int_{S^1\times\Omega}\chi_{C(\theta,\Delta\theta)}(p)d\mu=\frac{\Delta\theta}{2\pi}, \tag{27}$$

which does not depend on θ. Thus the quantum ergodicity theorem reads in the case of a characteristic function in momentum space

$$\lim_{j\to\infty}\int_{C(\theta,\Delta\theta)}|\hat{\psi}_{n_j}(p)|^2dp=\frac{\Delta\theta}{2\pi} \tag{28}$$

for a subsequence $\{n_j\}\subset\mathbf{N}$ of density one. This means that quantum ergodicity implies an asymptotic equidistribution of the momentum directions of the particle.

It is instructive to compute the observables discussed above for certain integrable systems. First consider a two-dimensional torus. The eigenfunctions, labeled by the two quantum numbers $n,m \in \mathbf{Z}$, read $\psi_{n,m}(x,y) = \exp(2\pi i n x)\exp(2\pi i m y)$. Obviously, these are ''quantum ergodic'' in position space since $|\psi_{n,m}(x,y)|^2 = 1$, but they are not quantum ergodic in momentum space. Even in position space the situation changes if one takes a different orthogonal basis of eigenfunctions (note that the multiplicities tend to infinity); see [32] for a discussion of the quantum limits on tori. A similar example is provided by the Dirichlet or Neumann eigenfunctions of a rectangular billiard.

The circle billiard shows a converse behavior. Let the radius be one; then the eigenfunctions are given in polar coordinates by

$$\psi_{kl}(r,\phi) = N_{kl} J_l(j_{k,l} r) e^{il\phi}. \tag{29}$$

Here $j_{k,l}$ is the kth zero of the Bessel function $J_l(x)$, $x>0$, and N_{kl} is a normalization constant. These eigenfunctions do not exhibit quantum ergodicity in position space. However, for their Fourier transforms one can show that

$$\int_{C(\theta,\Delta\theta)} |\hat{\psi}_{kl}(p)|^2 dp = \frac{\Delta\theta}{2\pi} \tag{30}$$

and so we have ''quantum ergodicity'' in momentum space.

A remarkable example was discussed by Zelditch [33]. He considered the Laplacian on the sphere S^2. Since the multiplicity of the eigenvalue $l(l+1)$ is $2l+1$, which tends to infinity as $l\to\infty$, one can choose infinitely many orthonormal bases of eigenfunctions. Zelditch showed that almost all of these bases exhibit quantum ergodicity in the whole phase space. Although this is clearly an exceptional case due to the high multiplicities, it shows that one has to be careful with the notion of quantum ergodicity. In a recent work Jakobson and Zelditch [34] have furthermore shown that for the sphere all invariant measures on phase space do occur as quantum limits. One might conjecture that for an integrable system all classical measures that are invariant under the flow and all symmetries of the Hamilton function do occur as quantum limits. The general question whether quantum ergodicity for all orthonormal bases of eigenfunctions in the whole phase space implies ergodicity of the classical system is still open.

D. Rate of quantum ergodicity

We now come to the central question of the approach to the quantum-ergodic limit. First we note that an equivalent formulation of the quantum ergodicity theorem, which avoids choosing subsequences, is given by

$$\lim_{E\to\infty} \frac{1}{N(E)} \sum_{E_n \le E} |\langle \psi_n, A\psi_n\rangle - \overline{\sigma(A)}| = 0. \tag{31}$$

This equivalence follows from a standard lemma concerning the influence of subsequences of density zero on the average of a sequence; see, e.g., [35], Theorem 1.20.

In order to characterize the rate of approach to the ergodic limit the quantities

$$S_m(E,A) = \frac{1}{N(E)} \sum_{E_n \le E} |\langle \psi_n, A\psi_n\rangle - \overline{\sigma(A)}|^m \tag{32}$$

have been proposed and studied in [13,14]. Quantum ergodicity is equivalent to $S_m(E,\mathrm{A})\to 0$ for $E\to\infty$ and $m \geqslant 1$.

Let us first summarize some of the known results for the rate of quantum ergodicity. Zelditch proved in [13] by relating the rate of quantum ergodicity to the rate of convergence of classical expectation values and using a central limit theorem for the classical flow that for compact manifolds of negative curvature $S_m(E,A) = O((\ln E)^{-m/2})$. However, this bound is believed to be far from being sharp. Moreover, in [14] lower bounds for $S_m(E,A)$ have been derived. In [15,36,37] it is proved for a Hecke basis of eigenfunctions on the modular surface that $S_2(E,A) < C(\varepsilon) E^{-1/2+\varepsilon}$ for every $\varepsilon > 0$. It is furthermore conjectured [6,15] that this estimate is also valid for the eigenfunctions of the Laplacian on a compact manifolds of negative curvature and moreover that it is satisfied for each eigenstate individually: $|\langle \psi_n, A\psi_n\rangle - \overline{\sigma(A)}| < C(\varepsilon) E^{-1/4+\varepsilon}$ for every $\varepsilon > 0$.

In [16] a study of $S_2(E,A)$ based on the Gutzwiller trace formula has been performed. For completely desymmetrized systems having only isolated and unstable periodic orbits, the so-called diagonal approximation for a double sum over periodic orbits and further assumptions lead to

$$S_2(E,A) \sim g \frac{2}{V(\Omega)} \rho(A) E^{-1/2}. \tag{33}$$

Here $g=2$ if the system is invariant under time reversal and otherwise $g=1$; $\rho(A)$ is the variance of the fluctuations of $A_\gamma = (1/T_\gamma)\int_0^{T_\gamma} \sigma(A)[\gamma(t)]dt$ around their mean $\overline{\sigma(A)}$, computed using all periodic orbits γ of the system. More precisely, it is assumed that $|A_\gamma - \overline{\sigma(A)}|^2 \sim \rho(A)/T_\gamma$, where T_γ denotes the primitive length of γ.

In the general case where not all periodic orbits are isolated and unstable it is argued that the rate of quantum ergodicity is related to the decay rate of the classical autocorrelation function $C(\tau)$ [16]. If $C(\tau) \sim \tau^{-\eta}$ then the result is

$$\begin{aligned} S_2(E,A) &\sim \int_0^{T_H} C(\tau) d\tau \\ &\sim \begin{cases} E^{-1/2} & \text{for } \eta > 1 \\ \ln\left(\dfrac{V(\Omega)}{2} E^{1/2}\right) E^{-1/2} & \text{for } \eta = 1 \\ E^{-\eta/2} & \text{for } \eta < 1, \end{cases} \end{aligned} \tag{34}$$

where $T_H = [V(\Omega)/2]E^{1/2}$ is the so-called Heisenberg time.

For the stadium billiard [38] and the Sinai billiard [39] it is believed that the correlations decay as $\sim 1/\tau$; see [40] and [41] for numerical results for the Sinai billiard. Thus, for both the stadium and the Sinai billiard a logarithmic contribution to the decay of $S_2(E,A)$ is expected. Also a Gaussian random behavior of the eigenfunctions [11] implies in position space a rate $S_2(E,A) = O(E^{-1/2})$, which follows from [42], Chap. IV; see also [16,43].

Random matrix theory (see [44], Sec. VII) predicts for suitable observables the same rate $S_2(E,A) = O(E^{-1/2})$ and

furthermore Gaussian fluctuations of $[\langle\psi_n, A\psi_n\rangle - \overline{\sigma(A)}]/\sqrt{S_2(E_n,A)}$ around zero, which we study numerically in Sec. III C.

Since for the systems under investigation we have non-quantum-ergodic subsequences of eigenfunctions, we now discuss in general the influence of such subsequences on the behavior of $S_1(E,A)$. To this end we split the sequence of eigenfunctions into two subsequences. The first, denoted by $\{\psi_{n'}\}$, contains all quantum-ergodic eigenfunctions, i.e., the corresponding quantum limit of the associated sequence of Wigner functions is the Liouville measure. The counting function of this subsequence will be denoted by $N'(E)$. The other sequence $\{\psi_{n''}\}$ contains all non-quantum-ergodic eigenfunctions. This subsequence may have different quantum limits μ_k that are all different from the Liouville measure. Their counting function will be denoted by $N''(E)$. Examples would be a subsequence of bouncing-ball modes or eigenfunctions scarred by an unstable periodic orbit. Similarly, we split $S_1(E,A)$ into two parts corresponding to the two classes of eigenfunctions. Due to the separation $N(E) = N'(E) + N''(E)$ we obtain

$$\begin{aligned} S_1(E,A) &= \frac{1}{N(E)} \sum_{E_n \leqslant E} |\langle\psi_n, A\psi_n\rangle - \overline{\sigma(A)}| \\ &= \frac{N'(E)}{N(E)} S_1'(E,A) + \frac{N''(E)}{N(E)} S_1''(E,A) \\ &= \left(1 - \frac{N''(E)}{N(E)}\right) S_1'(E,A) + \frac{N''(E)}{N(E)} S_1''(E,A). \end{aligned} \tag{35}$$

Here we defined

$$S_1'(E,A) := \frac{1}{N'(E)} \sum_{E_{n'} \leqslant E} |\langle\psi_{n'}, A\psi_{n'}\rangle - \overline{\sigma(A)}|, \tag{36}$$

$$S_1''(E,A) := \frac{1}{N''(E)} \sum_{E_{n''} \leqslant E} |\langle\psi_{n''}, A\psi_{n''}\rangle - \overline{\sigma(A)}|. \tag{37}$$

So the behavior of $S_1(E,A)$ is given in terms of the three quantities $S_1'(E,A)$, $S_1''(E,A)$, and $N''(E)$, which describe the behavior of the quantum-ergodic and the non-quantum-ergodic subsequences, respectively.

The behavior of $S_1''(E,A)$ can be described in terms of the non-quantum-ergodic limits and their counting functions. We split the non-quantum-ergodic subsequence into convergent subsequences corresponding to the quantum limits $\mu_k \neq \mu$, $\{\psi_{n''}\} = \cup_k \{\psi_{n_j^k}\}_{j \in \mathbf{N}}$, with $N''(E) = \Sigma_k N_k(E)$, and $\langle\psi_{n_j^k}, A\psi_{n_j^k}\rangle - \overline{\sigma(A)} \sim \mu_k(\sigma(A) - \overline{\sigma(A)})$. Then $S_1''(E,A)$ is asymptotically given by

$$S_1''(E,A) \sim \frac{1}{\sum_k N_k(E)} \sum_k N_k(E) |\mu_k(\sigma(A) - \overline{\sigma(A)})| \tag{38}$$

and the limit

$$\nu''(A) := \lim_{E \to \infty} S_1''(E,A) \tag{39}$$

depends only on $\sigma(A)$ and defines an invariant measure on Σ_1.

Let us assume for the quantum-ergodic part of $S_1(E,A)$ a certain rate of decay

$$S_1'(E,A) = \nu'(A) E^{-\alpha} + o(E^{-\alpha}) \tag{40}$$

and for the counting function of the non-quantum-ergodic states

$$N''(E) = cE^{\beta} + o(E^{\beta}), \tag{41}$$

where by quantum ergodicity $\alpha > 0$ and $\beta < 1$. With Weyl's law $N(E) = [V(\Omega)/4\pi]E + O(E^{1/2})$ we then obtain in Eq. (35) for $S_1(E,A)$

$$\begin{aligned} S_1(E,A) = \nu'(A) E^{-\alpha} + \frac{4\pi c}{V(\Omega)} \nu''(A) E^{\beta-1} + o(E^{-\alpha}) \\ + o(E^{\beta-1}). \end{aligned} \tag{42}$$

One sees that if $-\alpha > \beta - 1$, the asymptotic behavior of $S_1(E,A)$ is governed by the quantum-ergodic sequences of eigenfunctions, whereas in the opposite case $-\alpha \leqslant \beta - 1$, the non-quantum-ergodic sequences dominate the behavior asymptotically. Especially if $\beta - 1 > -1/4$, i.e., $\beta > 3/4$, the rate of quantum ergodicity cannot be $O(E^{-1/4})$.

To obtain a simple model for the rate of quantum ergodicity, let us now assume that the conjectured optimal rate is valid for the subsequence of quantum-ergodic eigenfunctions, that is, $\alpha = 1/4$ can be chosen in Eq. (40). To be more precise, it should be $S_1'(E,A) = O(E^{-1/4+\varepsilon})$ for every $\varepsilon > 0$, but for comparison with numerical data on a finite energy range we will assume that $\varepsilon = 0$. For the non-quantum-ergodic eigenfunctions the knowledge of their counting function $N''(E)$ is very poor; in general, it is unknown. Thus, if we neglect the higher-order terms in Eqs. (40) and (41) we obtain from Eqs. (35) and (39) a simple model for the behavior of $S_1(E,A)$,

$$\begin{aligned} S_1^{\text{model}}(E,A) = \left(1 - \frac{4\pi c}{V(\Omega)} E^{\beta-1}\right) \nu'(A) E^{-1/4} \\ + \frac{4\pi c}{V(\Omega)} \nu''(A) E^{\beta-1}. \end{aligned} \tag{43}$$

The first factor in large parentheses will only be important if β is close to 1.

Similar considerations can be made for $S_m(E,A)$, for $m > 1$, leading to

$$S_m(E,A) = \left(1 - \frac{N''(E)}{N(E)}\right) S_m'(E,A) + \frac{N''(E)}{N(E)} S_m''(E,A), \tag{44}$$

where $S_m'(E,A)$ and $S_m''(E,A)$ correspond to the quantum-ergodic and the non-quantum-ergodic part, respectively. They are defined as in Eqs. (36) and (37) with the mth powers of the absolute values instead of the absolute values themselves. To see the specific properties of the $S_m(E,A)$ for

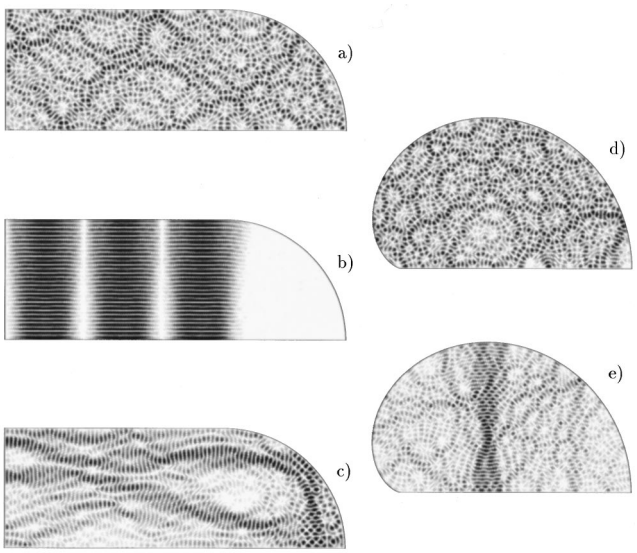

FIG. 1. Left: density plots $|\psi_n(q)|^2$ for three different odd-odd eigenfunctions of the $a=1.8$ stadium billiard: (a) $n=1992$, ''generic''; (b) $n=1660$, bouncing-ball mode; and (c) $n=1771$, localized eigenfunction. Right: density plots for two eigenfunctions of the cardioid billiard with odd symmetry: (d) $n=1816$, generic and (e) $n=1817$, localized along the $\overline{AB}$ orbit. Notice that according to the quantum ergodicity theorem, the nonlocalized eigenfunctions of type (a) and (d) are the overwhelming majority.

$m>1$ we study the special case that there is only one non-quantum-ergodic sequence $\{\psi_{n''}\}$ with quantum limit ν'' and that the rate for the quantum-ergodic sequence is proportional to $\nu'(A)E^{-1/4}$. Then one easily sees that $S''_m(E,A) \sim \nu''(A)^m$ and $S'_m(E,A)\sim[\nu'(A)^m/(1-m/4)]E^{-m/4}$ for $m<4$, $S'_m(E,A)\sim\nu'(A)^4 \ln(E)/E$ for $m=4$, and $S'_m(E,A) \sim E^{-1}$ for $m>4$. Therefore, by changing m one can change the relative weight of the quantum-ergodic and the non-quantum-ergodic contribution to S_m. The non-quantum-ergodic part gets more pronounced with larger m, but as will be discussed below, this effect can be hidden or even reversed on a finite-energy interval if $\nu''(A)\ll\nu'(A)$.

We will now discuss the influence of a special type of non-quantum-ergodic subsequences in more detail. In billiards with two parallel walls, one has a subsequence of so-called bouncing-ball modes [45], which are localized on the bouncing-ball orbits; see Fig. 1(b) for an example of such an eigenfunction. In [46] it was shown that for every $1/2<\beta<1$ there exists an ergodic billiard that possesses a non-quantum-ergodic subsequence, given by bouncing-ball modes, whose counting function is asymptotically of order E^β. However, for $\beta=1-\delta$, with some small $\delta>0$, Eq. (42) shows that $S_1(E,A)=O(E^{-\delta})$ at least for some A. So the best possible estimate of the rate of quantum ergodicity that is valid without further assumptions on the system other than ergodicity is

$$S_1(E,A)=o(1), \quad \text{i.e.,} \quad \lim_{E\to\infty} S_1(E,A)=0. \tag{45}$$

Especially for the Sinai billiard the result for the exponent is $\beta=9/10$ and therefore $S_1(E,A)\sim cE^{-1/10}$, which contradicts the result (34) from [16].

If the bouncing-ball modes are the only non-quantum-ergodic eigenfunctions or at least constitute the dominant contribution to them, then $N''(E)\sim N_{\mathrm{BB}}(E)\sim cE^\beta$. The exponent β and $\nu''(A)$ are explicitly known and the constant c is known from a numerical fit in [46] for the billiards we will consider in Sec. III. Thus, in this case the only free parameter in the model (43) is $\nu'(A)$.

The asymptotic behavior of Eq. (43) is governed by the term with the larger exponent, but this can be hidden at low energies if one of the constants is much larger than the other. Assume, for instance, that $\beta-1>1/4$, i.e., the non-quantum-ergodic eigenfunctions dominate the rate asymptotically. If

$$\frac{4\pi c\,\nu''(A)}{V(\Omega)\,\nu'(A)}\ll 1 \tag{46}$$

for an observable A, then up to a certain energy $S_1(E,A)$ will be approximately proportional to $E^{-1/4}$. In numerical studies where only a finite energy range is accessible such a behavior can hide the true rate of quantum ergodicity. This turns out to be the case for the cosine billiard; see Sec. III A 1. This effect gets even more pronounced for the $S_m(E,A)$ with $m>1$ because for $\nu''(A)/\nu'(A)<1$ one has $[\nu''(A)/\nu'(A)]^m<\nu''(A)/\nu'(A)$. Therefore, in such cases $S_1(E,A)$ seems to be the optimal choice for numerical studies.

The main ingredient of the model (43) is the conjectured behavior of the rate for the quantum-ergodic eigenfunctions. By comparing Eq. (43) with numerical data for different observables one can test this conjecture. If this conjecture is true then it means that the only deviations from the optimal rate of quantum ergodicity are due to subsequences of non-quantum-ergodic eigenfunctions.

Clearly, similar models based on a splitting such as Eq. (35) can be developed for other situations as well. For example, if the eigenfunctions split into a quantum-ergodic subsequence of density one with rate proportional to $E^{-1/4}$ and a quantum-ergodic subsequence of density zero with a slower, and maybe spatial inhomogeneous, rate, one would expect a similar behavior of $S_1(E,A)$ as in the case considered above. So it will be hard without some *a priori* information on non-quantum-ergodic eigenfunctions to distinguish between these two scenarios.

III. NUMERICAL RESULTS

In order to study the rate of quantum ergodicity numerically we have chosen three different Euclidean billiard systems, given by the free motion of a point particle inside a compact domain with elastic reflections at the boundaries. See Fig. 2 for the chosen billiard shapes.

The first is the stadium billiard, which is proven to be ergodic, mixing, and a K-system [38,47]. The height of the desymmetrized billiard is chosen to be 1 and a denotes the length of the upper horizontal line. For this system our analysis is based on computations of the first 6000 eigenfunctions for odd-odd parity, i.e., everywhere Dirichlet boundary conditions in the desymmetrized system with the parameter $a=1.8$. We also studied stadium billiards with parameters $a=0.5$ and $a=4.0$ using the first 2000 eigenfunctions in each case to investigate the dependence on a; see below. The

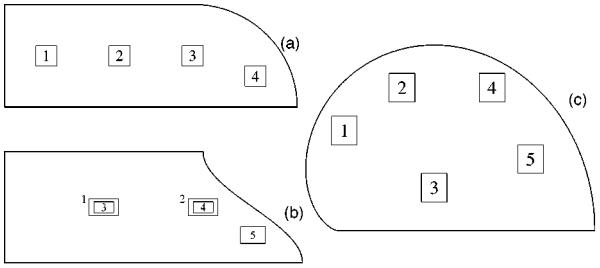

FIG. 2. Shapes of the billiards studied numerically in this work: (a) desymmetrized stadium billiard, (b) desymmetrized cosine billiard, and (c) desymmetrized cardioid billiard. The rectangles in the interior of the billiards mark the domains D_i of integration for studying the rate of quantum ergodicity in configuration space.

stadium billiard is one of the most intensively studied systems in quantum chaos; for investigations of the eigenfunctions see, e.g., [45,18,19,48,49] and references therein.

The second system is the cosine billiard, which is constructed by replacing one side of a rectangular box by a cosine curve. The cosine billiard has been introduced and studied in detail in [50,51]. The ergodic properties are unknown, but numerical studies do not reveal any stability islands. If there were any they are so small that one expects that they do not have any influence in the energy range under consideration. The height of the cosine billiard is 1 and the upper horizontal line has length 2 in our numerical computations. The cosine is parametrized by $B(y)=2+\frac{1}{2}[1+\cos(\pi y)]$; see Fig. 2(b). For our analysis of this system we used the first 2000 eigenfunctions with Dirichlet boundary conditions everywhere.

The third system is the cardioid billiard, which is the limiting case of a family of billiards introduced in [52]. The cardioid billiard is proven to be ergodic, mixing, a K-system, and a Bernoulli system [53–57]. Both the classical system [52,58–60] and the quantum-mechanical system have been studied in detail [61,62,58,63]. The eigenvalues of the cardioid billiard have been provided by Prosen and Robnik [64] and were calculated by means of the conformal mapping technique; see, e.g., [61,65,66]. Using these eigenvalues, our study is based on computations for the first 6000 eigenfunctions of odd symmetry, which were obtained from the eigenvalues by means of the boundary integral method [67,68] using the singular value decomposition method [69]. The boundary integral method was also used for the computations of the eigenvalues and eigenfunctions of the stadium and the cosine billiard.

Let us first illustrate the structure of wave functions by showing density plots of $|\psi_n(q)|^2$ for three different types of wave functions of the stadium billiard and two different types of the cardioid billiard. Figure 1(a) shows a ''generic'' wave function, whose density looks irregular. The example in Fig. 1(b) belongs to the class of bouncing ball modes and its Wigner function is localized in phase space on the bouncing ball orbits; see the discussion in Sec. II C. Figure 1(c) is another example of an eigenfunction showing some kind of localization. Figure 1(d) shows a generic wave function for the cardioid billiard and Fig. 1(e) is an example of an eigenfunction that shows a strong localization in the surrounding of the shortest periodic orbit (with code $\overline{AB}$; see [58,59]). We should emphasize that according to the quantum ergodicity theorem, the overwhelming majority of states in the semiclassical limit are of the type (a) and (d), which we also observe for the eigenfunctions of the studied systems.

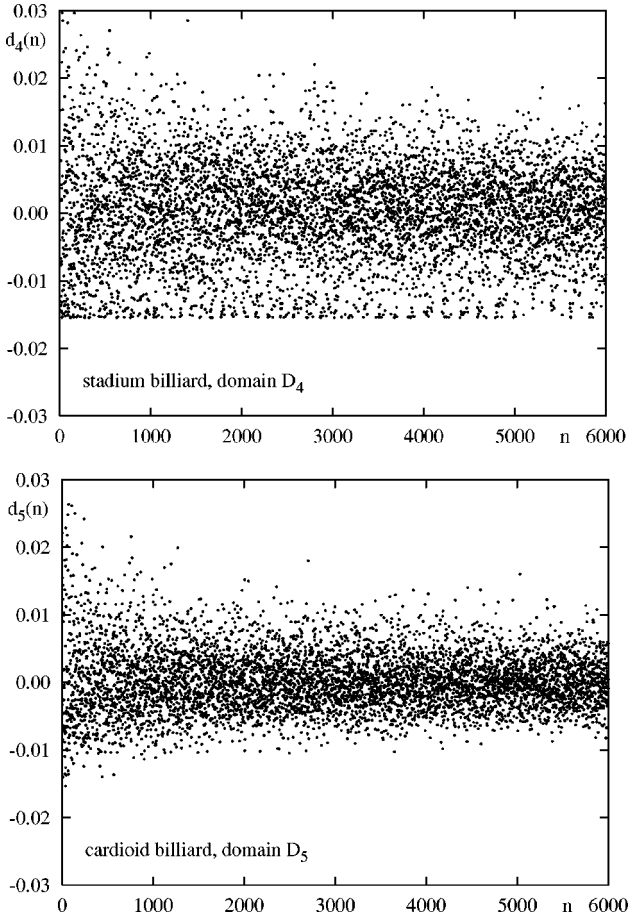

FIG. 3. Plot of $d_i(n)=\int_{D_i}|\psi_n(q)|^2dq-V(D_i)/V(\Omega)$ for domain 4 in the stadium billiard and for domain 5 in the cardioid billiard. Since $|\psi_n(q)|^2\geqslant 0$, one has $d_i(n)\geqslant -V(D_i)/V(\Omega)$. For domain D_4 in the stadium this lower bound is attained by the bouncing-ball modes whose probability density $|\psi_n(q)|^2$ nearly vanishes in D_4; they are responsible for the sharp edge seen in the plot of $d_4(n)$.

A. Quantum ergodicity in coordinate space

The quantum ergodicity theorem applied to the observable with symbol $a(q)=\chi_D(q)$, discussed in Sec. II C, states that the difference

$$d_i(n)=\int_{D_i}|\psi_n(q)|^2dq-\frac{V(D_i)}{V(\Omega)} \tag{47}$$

vanishes for a subsequence of density one. The first set of domains D_i for which we investigate the approach to the ergodic limit is shown in Fig. 2. Plots of $d_i(n)$ for domain D_4 of the stadium billiard and D_5 of the cardioid billiard in Fig. 3 show quite large fluctuations around zero. In particular, for the stadium billiard there are many states for which $d_1(n)$ is quite large and $d_4(n)$ is quite small. As one would expect, a large number of them are bouncing-ball modes. The fluctuations of $d_i(n)$ for the cosine billiard behave similarly to the stadium billiard.

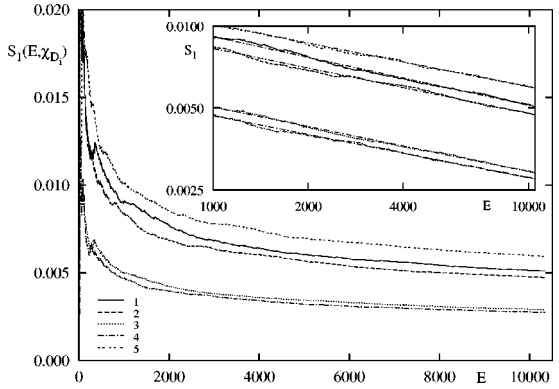

FIG. 4. Plot of $S_1(E,\chi_{D_i})$ for different domains D_i for the cosine billiard using the first 2000 eigenfunctions; see Fig. 2(b) for the location of the domains D_i. The inset shows the same curves in a double-logarithmic representation together with a fit of $S_1^{\mathrm{fit}}(E) = aE^{-1/4+\varepsilon}$ to the numerical data.

When trying to study the rate of the approach to the quantum-ergodic limit numerically one therefore is faced with two problems. On the one hand, $d_i(n)$ is strongly fluctuating, which makes an estimate of the approach to the mean very difficult, if not impossible for the available numerical data. On the other hand, one does not know *a priori* which subsequences should be excluded in Eq. (47). Therefore, the investigation of the asymptotic behavior of the ''cumulative'' version (31) of the quantum ergodicity theorem is much more appropriate. For the observable $\chi_D(q)$ we have

$$S_1(E,\chi_D) = \frac{1}{N(E)} \sum_{E_n \leqslant E} \left| \langle \psi_n, \chi_D \psi_n \rangle - \frac{V(D)}{V(\Omega)} \right|. \quad (48)$$

In Figs. 4–6 we display $S_1(E,\chi_{D_i})$ for the different domains D_i, shown in Fig. 2, in the desymmetrized cosine, stadium, and cardioid billiards, respectively. One clearly sees that the numerically determined curves for $S_1(E,\chi_{D_i})$ decrease with increasing energy. This is of course expected from the quantum ergodicity theorem; however, since this is an asymptotic statement, it is not clear *a priori* whether one can observe such a behavior also at low energies. It should be emphasized that Fig. 4 is based on the expectation values $\langle \psi_n, \chi_{D_i} \psi_n \rangle$ for 2000 eigenfunctions and Figs. 5 and 6 are based on 6000 eigenfunctions in each case.

In order to study the rate of quantum ergodicity quantitatively a fit of the function

$$S_1^{\mathrm{fit}}(E) = aE^{-1/4+\varepsilon} \quad (49)$$

to the numerical data for $S_1(E,\chi_{D_i})$ is performed. As discussed in Sec. II D, for certain systems a behavior $S_1(E,\mathrm{A}) = O(E^{-1/4+\varepsilon})$ for all $\varepsilon > 0$ is expected, so that the fit parameter ε characterizes the rate of quantum ergodicity. A positive value of ε thus means a slower decrease of $S_1(E,\mathrm{A})$ than the expected $E^{-1/4}$. The results for ε are shown in Tables I–IV, and the insets in Figs. 4–11 show the same curves $S_1(E,\chi_{D_i})$ in a double-logarithmic plot together with these fit curves. We find good agreement of the fits with the computed functions $S_1(E,\chi_{D_i})$. However, ε is not small for all domains D_i of the considered systems; rather we find several significant exceptions, which will be discussed in the following.

1. Cosine billiard

For the cosine billiard one would expect a strong influence of the bouncing-ball modes on the rate since their number increases according to [46] as $N_{\mathrm{BB}}(E) \sim cE^{9/10}$. However, the prefactor c turns out to be very small and therefore the influence of the bouncing-ball modes is suppressed at low energies. The model for $S_1(E,A)$ [Eq. (43)] gives for the cosine billiard

$$S_1^{\mathrm{model}}(E,\chi_{D_i}) = (1 - 0.201E^{-0.13})\,\nu'(\chi_{D_i})E^{-1/4} + 0.201\,\nu''_{\mathrm{BB}}(\chi_{D_i})E^{-0.13}, \quad (50)$$

where we have inserted the values $c = 0.04$ and $\beta = 0.87$, obtained in [46] from a fit to $N_{\mathrm{BB}}(E)$ that was performed over the same energy range that we consider here. For the sake of completeness we have included the first factor $(1 - 0.201E^{-0.13})$, but the numerical fits we perform below only change marginally if one sets this factor equal to 1.

The asymptotic behavior of the probability density $|\psi_{n''}(q)|^2$ of the bouncing-ball modes is (in the weak sense)

$$|\psi_{n''}(q)|^2 \sim \begin{cases} 1/V(R) & \text{for } q \in R \\ 0 & \text{for } q \in \Omega \backslash R \end{cases} \quad (51)$$

as $n'' \to \infty$, where R denotes the rectangular part of the billiard. So the expectation values are asymptotically $\langle \psi_{n''}, \chi_D \psi_{n''} \rangle \sim V(D \cap R)/V(R)$ and since $\nu''_{\mathrm{BB}}(\chi_D) = \lim_{E\to\infty} S''(E,\chi_D)$ is the mean value of $|\langle \psi_{n''}, \chi_D \psi_{n''} \rangle - V(D)/V(\Omega)|$ over all bouncing-ball modes one has

$$\nu''_{\mathrm{BB}}(\chi_D) = \left| \frac{V(D \cap R)}{V(R)} - \frac{V(D)}{V(\Omega)} \right|. \quad (52)$$

For fixed volume $V(D)$ the quantity $\nu''_{\mathrm{BB}}(\chi_D)$ is maximal for domains D lying entirely outside of the rectangular region $\nu''_{\mathrm{BB}}(\chi_D) = V(D)/V(\Omega)$. For domains lying entirely inside the rectangular part of the billiard, we have the minimal value $\nu''_{\mathrm{BB}}(\chi_D) = \frac{1}{4}[V(D)/V(\Omega)]$. Therefore, the strongest contribution of the bouncing-ball modes to $S_1(E,\chi_D)$ in Eq. (50) is expected for the domains outside the rectangular region.

The values for $\nu''_{\mathrm{BB}}(\chi_{D_i})$ are given in Table I. The largest values for the small domains are obtained for the domains outside the rectangular part of the billiard for which also the rate of quantum ergodicity is the slowest. Furthermore, we see from Table I that the factor $0.201\nu''_{\mathrm{BB}}(\chi_{D_i})$ in front of $E^{-0.13}$ in Eq. (50) is for all domains much smaller than the prefactor a from the fit to Eq. (49). This already indicates that the contribution of the bouncing-ball modes is suppressed, explaining why the rate for the cosine billiard is in such good agreement with $\varepsilon = 0$.

In order to test this quantitatively we have performed a fit of the model (50) to the numerical data, where the only free parameter is $\nu'(\chi_{D_i})$. The accuracy of the fits is very good and the results for $\nu'(\chi_{D_i})$ are shown in Table I; they are

TABLE I. Rate of quantum ergodicity for the cosine billiard with domains D_i as shown in Figs. 2 and 4 and in the inset of Fig. 7. Shown are the results for ε and a of the fit of $S_1^{\rm fit}(E) = aE^{-1/4+\varepsilon}$ to the numerical data. The values for the relative area of the corresponding domains, the quantities $\nu''_{\rm BB}(\chi_{D_i})$ computed according to Eq. (52), and the result $\nu'(\chi_{D_i})$ of the fit of the model (50) to $S_1(E,\chi_{D_i})$ are also tabulated.

Domain	Relative area	ε	a	$\nu'(\chi_{D_i})$	$\nu''_{\rm BB}(\chi_{D_i})$
1	0.018	−0.002	0.052	0.0525	0.0045
2	0.018	+0.012	0.026	0.0468	0.0067
3	0.008	+0.013	0.043	0.0297	0.0020
4	0.008	+0.022	0.023	0.0273	0.0030
5	0.015	+0.020	0.050	0.0543	0.0150
6	0.336	+0.009	0.258	0.2471	0.0840
7	0.512	+0.023	0.352	0.2920	0.1280
8	0.648	+0.009	0.381	0.3410	0.1620
9	0.800	+0.054	0.279	0.3264	0.2500

TABLE II. Rate of quantum ergodicity for the stadium billiard with domains D_i as shown in Figs. 2 and 8. Shown are the results for ε and a of the fit $S_1^{\rm fit}(E) = aE^{-1/4+\varepsilon}$ to $S_1(E,\chi_{D_i})$. The values for the relative area of the corresponding domains and the results $\nu'(\chi_{D_i})$ and $b(A)$ of the fit of the model (54) to $S_1(E,\chi_{D_i})$ are also tabulated.

Domain	Relative area	ε	a	$\nu'(\chi_{D_i})$	$b(A)$
1	0.015	+0.009	0.041	0.058	0.000
2	0.015	+0.012	0.041	0.059	0.000
3	0.015	+0.033	0.035	0.055	0.001
4	0.015	+0.095	0.029	0.046	0.006
5	0.015	+0.022	0.039	0.058	0.000
6	0.278	+0.125	0.082	0.112	0.034
7	0.433	+0.162	0.076	0.044	0.059
8	0.557	+0.172	0.086	0.011	0.080
9	0.696	+0.172	0.113	0.023	0.104
10	0.681	+0.092	0.164	0.257	0.035

much larger than the corresponding prefactors $0.201\nu''_{\rm BB}(\chi_{D_i})$ of the bouncing-ball part of $S_1(E,\chi_{D_i})$. Therefore, the influence of the bouncing-ball modes on the rate is negligibly small on the present energy interval, despite the fact that asymptotically they should dominate the rate.

The domains $D_3 \subset D_1$ and $D_4 \subset D_2$ show a slightly slower rate than D_1 and D_2, respectively. This is due to the fact that choosing a smaller domain D implies larger fluctuations of $\langle \psi_n, \chi_D \psi_n \rangle$ for the same set of eigenfunctions.

As an additional test we have computed $S_1(E,\chi_{D_i})$ numerically for four further domains (shown in the inset of Fig. 7) having a much larger area than the previous ones. For these domains $\nu''_{\rm BB}(\chi_{D_i})$ is larger and one therefore expects a stronger influence of the bouncing-ball modes and correspondingly a slower rate of quantum ergodicity. The results are shown in Table I and Fig. 7 and our findings are completely consistent with the previous one as well as with the model (50). We also observe in Fig. 7 that for the large domains, except for the whole rectangular part $D_9 = R$, the rate is faster at low energies than at high energies. This is due to the influence of the boundary and will be discussed in Sec. III A 4.

As discussed in Sec. II D, the influence of the bouncing-ball modes on the rate might be better visible in the behavior of the S_m for $m > 1$. However, since $\nu''_{\rm BB}(\chi_{D_i})$ is much smaller than $\nu'(\chi_{D_i})$ their influence is even stronger suppressed for $m > 1$ than for $m = 1$. We have computed the $S_m(E,\chi_D)$ numerically for different m and the different domains. For the small domains we found that the nonquantum-ergodic contribution is strongly suppressed, as expected. For the larger domains their influence is better visible, e.g., for D_9.

Summarizing the results for the cosine billiard, we found that the rate of quantum ergodicity is in impressive agreement with a rate proportional to $E^{-1/4}$ for the subsequence of quantum-ergodic eigenfunctions. The phenomenological model $S_1^{\rm model}(E,\chi_D)$ [Eq. (50)] is in good agreement with the numerical data, especially in view of the fact that it contains only one free parameter. Furthermore, the cosine billiard provides an interesting example of a system for which the asymptotic regime for $S_1(E,A)$ is reached very late. Up to the 2000th eigenfunction the asymptotic behavior $S_1(E,A) \sim CE^{-1/10}$ is almost completely hidden. A continuation of $S_1^{\rm model}(E,\chi_R)$ for the domain $R = D_9$ with the strongest influence of the bouncing-ball modes shows that at $E \approx 10^6$ the two contributions have the same magnitude and one has to go up as high as $E \approx 10^{20}$ to see the asymptotic behavior $S_1(E,\chi_R) \sim CE^{-1/10}$. Therefore there is no contradiction between the observed fast rate of quantum ergodicity in the present energy range and the increase of the number of bouncing-ball modes $N_{\rm BB}(E) \sim cE^{9/10}$ found in [46].

2. Stadium billiard

For the stadium billiard the number of bouncing-ball modes grows as $N_{\rm BB}(E) \sim cE^{3/4}$ [70,46]. Therefore, the bouncing-ball mode contribution to $S_1(E,A)$ is, according to Eq. (43), proportional to $E^{-1/4}$ and thus of the same order as the expected rate of quantum ergodicity for the quantum-ergodic eigenfunctions. One therefore expects for all domains in position space a rate of $E^{-1/4}$. We have investigated the rate of quantum ergodicity for the stadium billiard using the small domains shown in Fig. 2(a) and for larger domains shown in Fig. 8. The results of the fits of $S_1^{\rm fit}(E) = aE^{-1/4+\varepsilon}$ to the numerical data for $S_1(E,\chi_{D_i})$ are given in Table II.

Let us first discuss the rate for the small domains shown in Fig. 2(a). For the domains D_1 and D_2 that lie inside the rectangular part of the billiard the rate is in very good agreement with $E^{-1/4}$. However, both for the domain D_3 that lies on the border between the rectangular part and the quarter circle and in particular for domain D_4 that lies inside the quarter circle, one finds a slower rate than expected. This is a behavior that one would expect for a billiard with a much faster increasing number of bouncing-ball modes.

We see three possible explanations for this behavior of the rate for the stadium billiard.

(i) First, the counting function $N_{\rm BB}(E)$ for the bouncing-ball modes might increase with a larger exponent than 3/4,

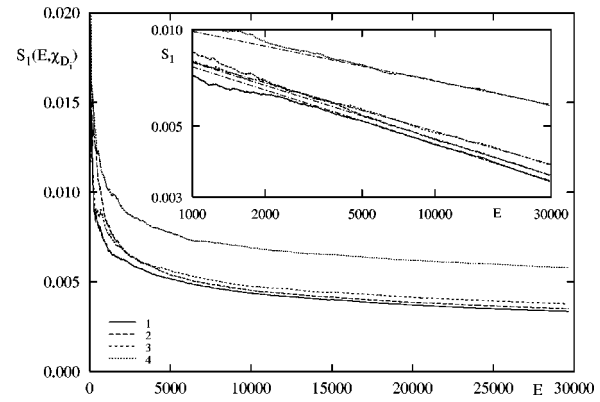

FIG. 5. Plot of $S_1(E,\chi_{D_i})$ for different domains D_i for the stadium billiard using the first 6000 eigenfunctions; see Fig. 2(a) for the location of the domains D_i. The inset shows the same curves in a double-logarithmic representation together with a fit of Eq. (49).

$N_{\mathrm{BB}}(E)\sim cE^{\beta}$, $\beta>3/4$. This would contradict the results in [70,46], derived by independent methods. Moreover, the exponent β was tested numerically in [46] up to energy $E\approx 10\,000$ and we found very good agreement with $\beta=3/4$. Even if we relaxed the criteria for the selection of the bouncing-ball modes drastically, the exponent did not change significantly; only the prefactor c increased. Therefore, we think that this first possibility is clearly ruled out.

(ii) Second, the rate for the quantum-ergodic eigenfunctions might not be proportional to $E^{-1/4}$, but has a slower decay rate. Then we have to assume a position dependence of the rate in order to explain the different behavior for the different domains: In the rectangular part of the billiard the rate has to be proportional to $E^{-1/4}$ to explain the value of ε obtained for the domains D_1 and D_2, whereas inside the quarter circle the rate of decay has to decrease as $S_1'(E,\chi_{D_4})\sim\nu'(A)E^{-0.15}$ in order to explain the value of ε obtained for D_3 and D_4. *A priori* such a dependence of the rate of the quantum-ergodic eigenfunctions on the location of the domain in the billiard is not impossible. If this is the case then one should observe no dependence of the rate on the volume of the domain D, as long as one stays in the same region of the billiard. For example, the rate for a domain such as D_6, which contains D_1 and D_2 and is far enough away from the quarter circle, should be the same as the one for D_1 and D_2.

(iii) The third possible explanation for the observed behavior of the rate is that there exist more non-quantum-ergodic eigenfunctions that have a larger probability density in the rectangular part than in the quarter circle and are not bouncing-ball modes. Alternatively, the reason could be a subsequence of density zero of quantum-ergodic eigenfunctions, which has a sufficiently increasing counting function and a slow rate; see the remark at the end of Sec. II D. In both cases the model for $S_1(E,A)$ discussed in Sec. II D, which we already used in the case of the cosine billiard, would be applicable. In contrast to the second possibility in this scenario, one expects a dependence of the rate of $S_1(E,\chi_D)$ on the volume of the domain D, as in the case of the cosine billiard.

To decide which explanation is the correct one we studied the rate for a number of domains with different area and located at different regions in the billiard. A selection of them is shown in Fig. 8. With the larger domains one necessarily comes closer to the boundary of the billiard. To rule out the possibility that the observed behavior of the rate is due to the influence of the boundary and not due to the dependence on the volume and location of the domains, we computed in addition $S_1(E,\chi_D)$ for the small domain D_5 that is close to the boundary.

The results are also given in Table II and some examples of $S_1(E,\chi_{D_i})$ for these large domains are shown in Fig. 9. As for the cosine billiard, we also found that for large domains at small energies the rate may be much faster than at higher energies, which is clearly seen in Fig. 9 for the domains D_7 and D_8. This effect is due to the influence of the boundary, as we will discuss in Sec. III A 4; here we only note that the boundary influence vanishes for large energies.

The observed rate of quantum ergodicity displays a strong dependence on the volume of the domain D, whereas the location, as long as one stays inside the rectangular part, has no influence. For example, for the domain D_6, which contains D_1 and D_2, one gets a much slower rate than for D_1 and D_2. In contrast to D_6, the rate for the small domain D_5 near the boundary is rather close to the one for D_1 and D_2. The slightly slower rate for D_5 is due to the smaller energy range for which we have computed $S_1(E,\chi_{D_5})$. A fit of $S_1^{\mathrm{fit}}(E)=aE^{-1/4+\varepsilon}$ to $S_1(E,\chi_{D_1})$ and $S_1(E,\chi_{D_2})$ using the first 2000 eigenfunctions gives an ε of 0.022 for D_1 and 0.011 for D_2, which is of the same magnitude as the result for D_5. Moreover, the rate decreases monotonically with increasing area of the domains D_i, as long as they are inside the rectangular part R of the billiard.

The domain D_{10} is interesting because it extends over both parts of the billiard. The enhanced probability density of the exceptional eigenfunctions in the rectangular part is partially compensated by the lower probability density in the quarter circle. Therefore one expects a rate similar to a domain in the rectangular part with relative area $\{V(D_{10})-2V[D_{10}\cap(\Omega\backslash R)]\}/V(\Omega)=0.371\ldots$. This relative area lies between the values for D_6 and D_7 and indeed the rate for D_{10} lies between the rate for D_6 and D_7 too.

These results strongly support the third explanation, i.e., the existence of a large density zero subsequence that is responsible for the deviations of the rate from $E^{-1/4}$. ''Large'' means that the counting function increases sufficiently strongly to cause the rate to deviate from the expected behavior. A lower bound on this counting function is given according to Eq. (42) by the slowest rate that is observed. For the stadium billiard this is the one for D_9, which leads to $N''(E)\gtrsim E^{0.92}$.

To test this conjecture quantitatively one has to compare the numerical data with the conjectured behavior

$$S_1^{\mathrm{model}}(E,A)=(1-cE^{-\beta})\nu'(A)E^{-1/4}+b(A)E^{-\beta}. \tag{53}$$

Since this model contains the four free parameters c, β, $\nu'(A)$, and $b(A)$, the numerical fit is not very stable. Therefore, it is desirable to get some additional information from a different source.

To this end we plotted $d_9(n)=\langle\psi_n,\chi_{D_9}\psi_n\rangle - V(D_9)/V(\Omega)$ for domain D_9, which is the whole rectangular part and shows a slow rate; see Fig. 3. Then we divided the spectrum into two parts by inserting a horizontal line γ, $\gamma>0$. The part of the spectrum above the line corresponds to the non-quantum-ergodic eigenfunctions whose quantum limits satisfy $\nu(\chi_{D_9})\geqslant|D_9|+\gamma$. From this we obtained for the counting function of the non-quantum-ergodic subsequence $N''(E)=0.08E^{0.93}$. This allows us to determine the parameters $c=0.08[4\pi/V(\Omega)]=0.39\ldots$ and $\beta=-0.07$ in the model (53) giving

$$S_1^{\text{model}}(E,A)=(1-0.39E^{-0.07})\,\nu'(A)E^{-1/4}+b(A)E^{-0.07}. \tag{54}$$

We have now eliminated two of the four free parameters and can therefore test this formula with the numerical data. The results for $\nu'(\chi_{D_i})$ and $b(\chi_{D_i})$ are also shown in Table II and for three large domains the plot of $S_1(E,\chi_D)$ and the corresponding fit $S_1^{\text{model}}(E,\chi_D)$ is shown in Fig. 9.

The agreement of the fits with the numerical data is good. Moreover, the values for $\nu'(D_i)$ and $b(D_i)$ are reasonable: The behavior of $b(D_i)$ is in accordance with what one expects for a sum of quantum limits that are concentrated on the rectangular part of the billiard. The values increase when moving D_i into the quarter circle and they increase with increasing volume of D_i, as long as D_i lies entirely inside the rectangular part. For D_{10} the parameter $b(D_{10})$ takes an intermediate value between $b(D_6)$ and $b(D_7)$, as one expects from our model. Varying the parameter γ that governs the selection of the non-quantum-ergodic subsequence, and therefore $N''(E)$, leads only to slight variations of the coefficients $\nu'(D_i)$ and $b(D_i)$. Due to the presence of c in front of $\nu'(D_i)$ in Eq. (54), the variations of $\nu'(D_i)$ are larger than those of $b(D_i)$.

The inclusion of the factor $1-0.39E^{-0.07}$ in Eq. (54) turned out to be necessary to get satisfactory results. The contribution of $E^{-0.07}$ cannot be neglected in the present energy range because of the small exponent. Without this factor we obtained for some of the domains negative values for $\nu'(D_i)$, which is impossible because $S_1'(E,A)$ is by definition positive. This also sheds some light on the limitations of such a simple model like (54). Nothing is known about the behavior of the higher-order contributions to $S_1'(E,A)$ and $S_1''(E,A)$. In view of this, it is surprising how good this model fits with the numerical data. We believe that this gives strong support for the underlying conjectures, namely, that a density one subsequence of quantum-ergodic eigenfunctions has a rate $S_1'(E,A)\sim cE^{-1/4}$ and the deviations in the rate of $S_1(E,A)$ from this behavior are due to a subsequence of density zero.

As mentioned in Sec. II D, a behavior $S_2(E,A)\sim cE^{-1/2}\ln\{[V(\Omega)/2]E^{1/2}\}$ for the stadium billiard is claimed in [16]. We have tested this both for the small domains D_1 and D_2, which are not influenced by the bouncing-ball modes, and also for some larger domains. However, the resulting fits clearly show that this result does not apply to our numerical data; see Fig. 10. We also tested if this result applies to the quantum-ergodic subsequence, i.e., $S_1'(E,A)\sim cE^{-1/4}\sqrt{\ln\{[V(\Omega)/2]E^{1/2}\}}$, by replacing the term $E^{-1/4}$ in the model (54) by $E^{-1/4}\sqrt{\ln\{[V(\Omega)/2]E^{1/2}\}}$. Again we find that from our numerical data that this possibility is excluded, at least for the energy range under consideration. For the stadium billiard it is known that the asymptotic behavior of the classical autocorrelation $C(\tau)\sim 1/\tau$, which leads to $S_2(E,A)\sim cE^{-1/2}\ln\{[V(\Omega)/2]E^{1/2}\}$ according to [16], sets in rather late. So it would be very interesting to compare the results with those obtained by inserting the numerically computed autocorrelation function in the integral in Eq. (34).

TABLE III. Results for ε of the fit of $S_1^{\text{fit}}(E)=aE^{-1/4+\varepsilon}$ to the numerically obtained $S_1(E,\chi_{D_i})$, for stadium billiards with different parameter a for three different domains A, B, and C. Domain A lies within the rectangular part of the billiard, domain B is centered at $x=a$, and domain C is located in the quarter circle.

System	Domain A	Domain B	Domain C
stadium ($a=0.5$)	$+0.111$	$+0.062$	$+0.056$
stadium ($a=1.8$)	$+0.009$	$+0.033$	$+0.095$
stadium ($a=4.0$)	-0.008	$+0.031$	$+0.095$

We now return to the question of what type these additional subsequences of eigenfunctions are. As additional information for the model, the counting function for the number of states for which $\langle\psi_n,\chi_{D_9}\psi_n\rangle - V(D_9)/V(\Omega)$ is smaller than $-\gamma$ has been used. For comparison we have carried out the same procedure for the observable χ_{D_4} that lies under the quarter circle. As expected, the bouncing-ball modes appeared in both subsequences, but additionally a considerable number of other types of eigenfunctions show up. In Fig. 11 we show some examples of such eigenfunctions. They all show a reduced probability density inside the quarter circle, but their structure is essentially different from the bouncing-ball modes. Their semiclassical origin are maybe periodic orbits bouncing up and down between the two perpendicular walls for a long time but then leaving the neighborhood of the bouncing-ball orbits in phase space. At least it seems difficult to associate short unstable periodic orbits with the patterns in the shown states because the lines of enhanced probability do not always obey the laws of reflection or they look too irregular.

A further test of the hypothesis that a density zero subsequence is responsible for the slow rate is provided by varying the length a of the billiard. Here we used the first 2000 eigenfunctions for both the $a=0.5$ and the $a=4.0$ stadium billiard in addition to the results for the $a=1.8$ stadium based on 6000 eigenfunctions. We have chosen three different domains for these three systems: domain A lies within the rectangular part of the billiard, domain B is centered at $x=a$, and domain C is located in the quarter circle. The results for the rate of quantum ergodicity are shown in Table III. For different parameters the quantities $b(D_i)$ change and therefore the weights of the different contributions to $S_1(E,A)$ in Eq. (54). For smaller a the relative fraction of the volume of the rectangular part, $V(R)/V(\Omega)$ becomes smaller. Therefore, one expects that for smaller a the influence of the non-quantum-ergodic subsequences to $S_1(E,\chi_D)$ becomes stronger in the rectangular part and weaker in the

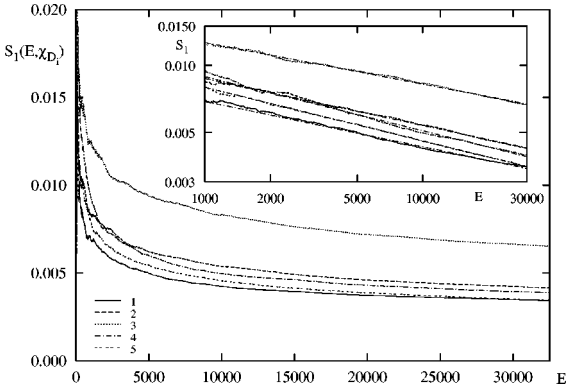

FIG. 6. Plot of $S_1(E,\chi_{D_i})$ for different domains D_i for the cardioid billiard using the first 6000 eigenfunctions; see Fig. 2(a) for the location of the domains D_i. The inset shows the same curves in a double-logarithmic representation together with a fit of $S_1^{\mathrm{fit}}(E) = aE^{-1/4+\varepsilon}$, [Eq. (49)].

quarter circle. This is clearly seen in the numerically found behavior of the rate for the domains A and C shown in Table III.

To summarize our results for the stadium billiard, we have given numerical evidence for the existence of a large, but density zero, subsequence of eigenfunctions that have an enhanced probability distribution on the rectangular part of the billiard but a different structure from the bouncing-ball modes. We demonstrated that the observed effects can be explained with the influence of this subsequence of density zero. This subsequence shows a different behavior from the majority of quantum-ergodic eigenfunctions for which our results imply a uniform rate of $E^{-1/4}$. Clearly, we cannot decide if this exceptional subsequence will ultimately be non-quantum-ergodic or if it is a quantum-ergodic subsequence with an exceptional behavior of the rate. We can only say that on the presently studied energy range up to $E \approx 30\,000$, i.e., up to the 6000th eigenfunction, they behave non-quantum-ergodically.

3. Cardioid billiard

The cardioid billiard is probably the most generic one of our three billiards, in the sense that it possesses no two-dimensional family of periodic orbits like the bouncing-ball

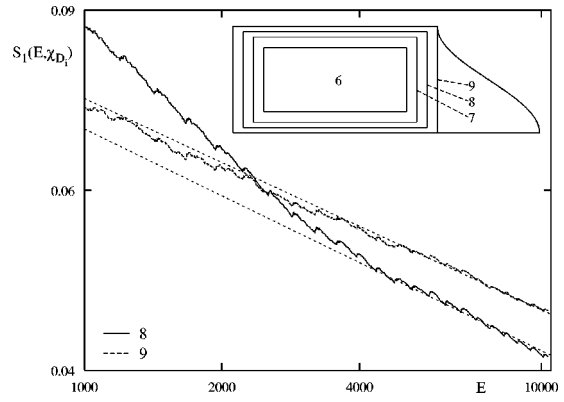

FIG. 7. Plot of $S_1(E,\chi_{D_i})$ for two further domains D_8 and D_9 (dashed curve) in the cosine billiard using the first 2000 eigenfunctions. Also shown is the fit $S_1^{\mathrm{model}}(E,\chi_{D_i})$ [Eq. (50)].

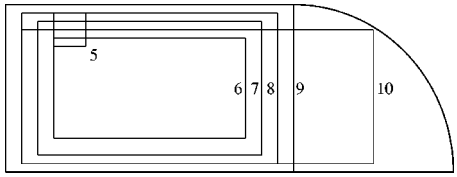

FIG. 8. Domains in the $a=1.8$ stadium billiard used to decide between the different explanations for the slow rates in the stadium billiard.

orbits. One might therefore expect *a priori* a better rate of quantum ergodicity than for the other billiards.

We have computed $S_1(E,\chi_{D_i})$ for five small domains [see Fig. 2(c)] by using the first 6000 eigenfunctions up to energy $E \approx 32\,000$ and for three larger domains (see Fig. 12) by using the first 2000 eigenfunctions. The results are displayed in Figs. 6 and 12. To determine the rate a fit of $S_1^{\mathrm{fit}}(E) = aE^{-1/4+\varepsilon}$ has been performed and the resulting values for a and ε are listed in Table IV.

We find that domain D_3 gives the lowest rate of quantum ergodicity for the small domains D_1–D_5. This is caused by a considerable number of eigenfunctions showing an enhanced probability as in Fig. 1(e) along the vertical orbit $\overline{AB}$. For domains D_1, D_2 we also find a slower rate than for the other regions D_4, D_5; in this case the slower rate seemingly cannot be attributed to one type of localized eigenfunctions.

The larger domains show a slower rate than the small domains, but the rate is not monotonically decreasing with the area of the domain. The rate for the largest domain D_8 is even of the same order of magnitude as the one for D_3, especially if one takes the smaller energy range for D_8 into account. This slower rate is probably caused by the existence of different non-quantum-ergodic subsequences with quantum limits μ_k in different regions of the billiard. For each of the domains the influence of these subsequences is different and therefore one observes different rates.

A quantitative test in a way similar to that for the other billiards using a model for $S_1(E,A)$ is very difficult because the deviations from the conjectured optimal rate is not only

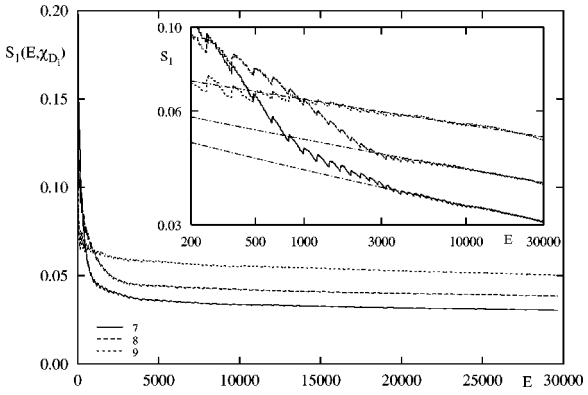

FIG. 9. Plot of $S_1(E,\chi_D)$ for large domains (see Fig. 8) for the $a=1.8$ stadium billiard using the first 2000 eigenfunctions. The inset shows the same curves in a double-logarithmic representation together with a fit of Eq. (49). For the domains D_7 and in particular for domain D_8 a sharp transition from a fast to a slower decay of the rate is visible. This effect is due to the boundary and will be explained in Sec. III A 4.

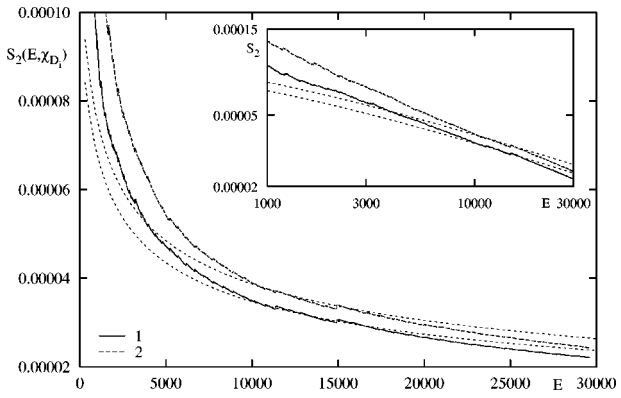

FIG. 10. Plot of $S_2(E,\chi_{D_i})$ for the domains D_1 and D_2 in the stadium billiard. The dashed lines show the fit of the conjectured behavior $cE^{-1/2}\ln\{[V(\Omega)/2]E^{1/2}\}$ to $S_2(E,\chi_{D_i})$. The result of the fit shows that the numerical data for the first 6000 expectation values cannot be described with this rate.

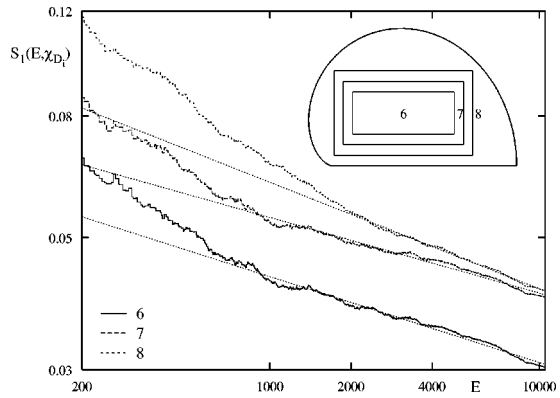

FIG. 12. Plot of $S_1(E,\chi_{D_i})$ for larger domains for the cardioid billiard using the first 2000 eigenfunctions. Also shown are fits to Eq. (49) for the corresponding energy regions.

due to one subsequence. However, the results for D_4 and D_5 clearly shows that here as well one has a density one subsequence of quantum-ergodic eigenfunctions with rate $S_1'(E,\chi_D)\sim\nu'(D)E^{-1/4}$. We hope to return to the problem of determining the non-quantum-ergodic subsequences and their quantum limits in the future.

The cardioid billiard is the only system we have studied to which the result (33) should be applicable. However, for most of the domains the rate is much slower than the predicted one. Only the domains 4 and 5 show the expected rate. Therefore, we have computed for these domains the factor $\rho(A)$ in Eq. (33). For the computation of $\rho(A)$ the variance of $\langle\chi_{D_i}\rangle_l - V(D_i)/V(\Omega)$ as a function of l has been computed using trajectory segments of length l of a generic trajectory $\{q(t)\}$. The quantity $\langle\chi_{D_i}\rangle_l=(1/l)\int_0^l\chi_{D_i}[q(t)]dt$ is the relative length of the trajectory segment lying in the domain D_i. By ergodicity we have $\lim_{l\to\infty}\langle\chi_{D_i}\rangle_l = V(D_i)/V(\Omega)$. The variance of $\langle\chi_{D_i}\rangle_l - V(D_i)/V(\Omega)$ decreases like $\rho(A)l^{-1}$.

Using the corresponding results in Eq. (33), we obtain $S_2(E,\chi_{D_4})=0.0062E^{-1/2}$ and $S_2(E,\chi_{D_5})=0.0074E^{-1/2}$. These numbers have to be compared with the result of a fit $S_2^{\rm fit}(E,A)$ to $S_2(E,\chi_{D_i})$. We obtain $S_2^{\rm fit}(E,\chi_{D_4}) = 0.0036E^{-0.47}$ and $S_2^{\rm fit}(E,\chi_{D_5})=0.0031E^{-0.48}$. One sees that the theoretical prediction is too large by a factor of approximately 2. This deviation might be related to the factor g in Eq. (33), which counts the mean multiplicities in the classical length spectrum. In the cardioid billiard the asymptotic value $g=2$ is reached very late; for the shorter periods one rather has $g\approx 1$, which would lead to a better agreement of Eq. (33) with the data for D_4 and D_5.

For a better understanding it seems necessary to check in detail whether any of the assumptions leading to Eq. (33) are not fulfilled for the domains of the cardioid billiard. It would also be very interesting to investigate if the slower rates can be described using the expression in terms of the classical correlation function. We will leave these questions for a separate study.

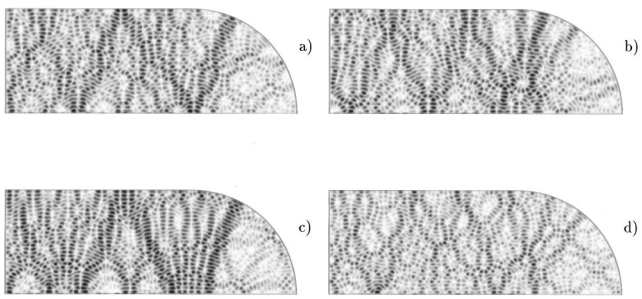

FIG. 11. Four examples of the exceptional eigenfunctions showing localization in the rectangular part of the stadium billiard, which are not bouncing-ball modes: (a) $n=1643$, (b) $n=1652$, (c) $n=1797$, and (d) $n=1834$.

4. Influence of the boundary

In all three billiards we observe the phenomenon that for large domains $S_1(E,\chi_D)$ decays faster at low energies than at high energies. This can be seen in Fig. 7 for domain D_8 in the cosine billiard, in Fig. 9 for domains D_7 and D_8 in the stadium billiard, and in Fig. 12 for domains D_6, D_7, and D_8 in the cardioid billiard. The other large domains we studied showed the same behavior. The only exceptions are the domains D_9 in the cosine billiard and in the stadium billiard, which consist of the whole rectangular part. For these domains no faster rate at low energies is visible.

Qualitatively this behavior can be understood by the vanishing of the probability density $|\psi_n(q)|^2$ of the eigenstates

TABLE IV. Rate of quantum ergodicity obtained from a fit of $S_1^{\rm fit}(E)=aE^{-1/4+\varepsilon}$ to $S_1(E,\chi_{D_i})$ for the cardioid billiard with domains D_i as shown in Figs. 2(a) and 12.

Domain	Relative area	ε	a
1	0.01722	+0.047	0.028
2	0.01722	+0.039	0.037
3	0.01722	+0.064	0.046
4	0.01722	+0.007	0.048
5	0.01722	+0.009	0.042
6	0.18674	+0.098	0.125
7	0.33104	+0.115	0.140
8	0.50930	+0.071	0.213

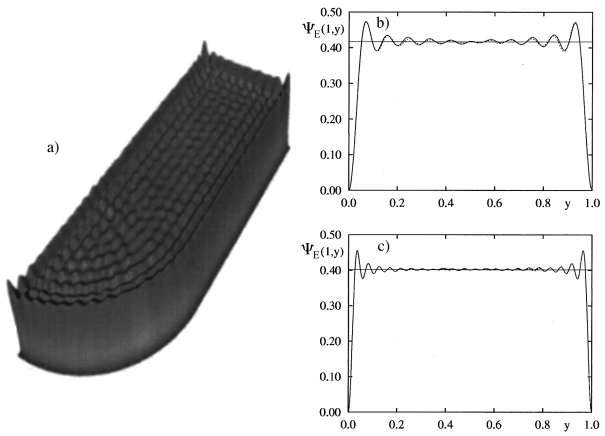

FIG. 13. In (a) we show a three-dimensional plot of the sum $\Psi_E(x,y)=[1/N(E)]\Sigma_{E_n\leqslant E}|\psi(x,y)|^2$ involving the first 250 eigenfunctions of the $a=1.8$ stadium with odd-odd symmetry. The pictures on the right show a cross section $\Psi_E(1,y)$ for using the first (b) 250 and (c) 1000 eigenfunctions. The dashed curves in (b) and (c) display the evaluation using the first two terms in formula (55). These results are used to explain the fast rate in the low-energy range for the stadium billiard for large domains.

at the boundary due to the Dirichlet boundary conditions. Because of the normalization of $\psi_n(q)$, the reduced probability density at the boundary has to be compensated by an enhancement of the probability density inside the billiard, which leads to larger oscillations of the probability density near the boundary.

Let us assume that this compensation of the probability density takes place in a strip along the boundary with a width of a few de Broglie wavelengths. Then the integral of the probability density $|\psi_n(q)|^2$ over a domain D ''feels'' the influence of the boundary only up to a certain energy, proportional to the inverse square of the distance between D and the boundary $\partial\Omega$. Furthermore, the boundary influence will be proportional to the overlap of D and the strip at the boundary. This overlap decreases like $1/\sqrt{E_n}$ and therefore $S_1(E,\chi_D)$ should decrease with such a rate at low energies. So the assumption that the compensation takes place in a small strip along the boundary leads exactly to the behavior we observe. Moreover, a domain like D_9 that extends to the boundary $\partial\Omega$ will not feel any influence because the boundary effect is compensated entirely inside this domain.

To justify our assumption on the range of the boundary influence we refer to the following result on the asymptotic behavior of the summed probability densities on a two-dimensional Riemannian manifold with a C^∞ boundary (see [20], Theorem 17.5.10):

$$\sum_{E_n\leqslant E}|\psi_n(q)|^2=\frac{1}{4\pi}E-\frac{1}{4\pi}\frac{J_1[2d(q)\sqrt{E}]}{d(q)}\sqrt{E}+R(q,E), \tag{55}$$

where $d(q)$ is the shortest distance of the point $q\in\Omega$ to the boundary. The remainder $R(q,E)$ satisfies the estimate $|R(q,E)|\leqslant C\sqrt{E}$. The second term in Eq. (55) describes the influence of the boundary; for $d(q)\to 0$ the term tends to $-E/(4\pi)$ and cancels the contribution from the first term such that the boundary conditions are fulfilled. In Fig. 13(a) the normalized sum

$$\Psi_E(x,y)=\frac{1}{N(E)}\sum_{E_n\leqslant E}|\psi_n(x,y)|^2, \tag{56}$$

is displayed for the stadium billiard, using the first 250 eigenfunctions. One clearly sees how the probability density is forced to vanish at the boundary and how the compensation leads to large oscillations near the boundary. In Figs. 13(b) and 13(c) we show two cross sections through the function (56) at two different energies and compare it to the result one gets from the first two terms on the right-hand side of Eq. (55). The agreement is quite impressive, especially near the boundary ($y=0$ and $y=1$). So although the stadium billiard does not have a C^∞ boundary, the result (55) seems to remain valid. One furthermore observes that with higher energies the y range on which the agreement is excellent increases.

The averaged probability density (56) shows exactly the behavior we assumed for the individual wave functions in order to explain the fast rate of quantum ergodicity at low energies for domains near the boundary. The influence of the Dirichlet boundary condition is concentrated near the boundary and it decays at a length scale proportional to the de Broglie wavelength. So with the help of Eq. (55) one gets a good qualitative understanding of the boundary influence on the rate of quantum ergodicity.

In order to try to get a quantitative understanding we used Eq. (55) to derive as in [17] a mean eigenfunction that incorporates the boundary influence

$$|\psi_n(q)|^2\approx\frac{1}{V(\Omega)-\dfrac{V(\partial\Omega)}{2\sqrt{E_n}}}\{1-J_0[2d(q)\sqrt{E_n}]\}. \tag{57}$$

Integrating this expression over a domain D should give for the expectation values the mean value plus the corrections due to the boundary of χ_D. By incorporating this into $S_1(E,\chi_D)$ one obtains an expression, which we compared with our numerical data. Although Eq. (57) implies a faster decay rate at low energies, it is not as strong as the numerically observed one. This deviation must be caused by considerable fluctuations of the boundary influence on the individual states ψ_n around the mean influence described by Eqs. (55) and (57).

B. Quantum ergodicity in momentum space

Up to here we have investigated the behavior of the wave functions in position space only. Now we turn our attention to the rate of quantum ergodicity in momentum space, which is studied here numerically.

Quantum ergodicity predicts that the angular distribution of the momentum probability distribution $|\hat{\psi}_n(p)|^2$ tends to $1/2\pi$ in the weak sense; see Eq. (28). Therefore, we study an observable with symbol $\chi_{C(\theta,\Delta\theta)}(p)$ whose expectation value gives the probability of finding the particle with momentum direction in the interval $]\theta-\Delta\theta/2,\theta+\Delta\theta/2[$. Recall that $\chi_{C(\theta,\Delta\theta)}(p)$ denotes the characteristic function of the circular sector $C(\theta,\Delta\theta)=\{p\in\mathbf{R}^2|\arctan(p_y/p_x)\in]\theta$

$-\Delta\theta/2, \theta+\Delta\theta/2[\}$ and the classical mean value of $\chi_{C(\theta,\Delta\theta)}(p)$ is $\Delta\theta/2\pi$.

Only eigenfunctions of odd parity of the nondesymmetrized systems are considered here due to our method of computing the Fourier transformation directly from the normal derivative $u_n(\omega)$ of the eigenfunction $\psi_n(q)$. From Green's theorem one easily finds the formula

$$\hat{\psi}_n(p) = \frac{1}{p^2 - E_n} \frac{1}{2\pi} \int_{\partial\Omega} e^{-iq(\omega)p} u_n(\omega) d\omega, \qquad (58)$$

where $q(\omega)$ denotes a point on the boundary $\partial\Omega$. The advantage of this formula is that it allows one to compute the Fourier transform directly from $u_n(\omega)$, which can be obtained using the boundary integral method. For desymmetrized systems, like the ones considered here, one uses an appropriate Green's function that vanishes at the lines of symmetry and therefore removes them from the boundary integral; see, e.g., [71]. This reduces the computational effort, but one does not get the normal derivatives on these parts of the boundary of the desymmetrized system. Therefore, our results for the rate of quantum ergodicity in momentum space are sufficient to rule out the possibility of a totally different behavior in momentum space than in position space. Since the rate for all eigenfunctions cannot be faster than the one for a subsequence of positive density, we get a lower bound for the rate of the full system.

The time-reversal invariance leads, for the Fourier-transformed eigenfunctions, to the symmetry $\hat{\psi}_n(-p) = \overline{\hat{\psi}_n(p)}$. Therefore, $|\hat{\psi}_n(-p)|^2 = |\hat{\psi}_n(p)|^2$ and this reduces the angle interval we have to study to $[0,\pi[$. The additional reflection symmetries in the considered billiards further reduce the relevant angle interval to $[0,\pi/2[$.

For our numerical computations we have chosen five equidistant intervals, centered at $\theta_i = (i-1/2)(\pi/10)$ with $i = 1,\ldots,5$ of width $\Delta\theta = \pi/10$. As in the case of quantum ergodicity in coordinate space [see Eq. (47) and Fig. 3], one observes large fluctuations of $\langle \psi_n, \chi_{C(\theta,\Delta\theta)}\psi_n\rangle - \Delta\theta/(2\pi)$ around 0. Therefore, we again consider the cumulative version (31) of the quantum ergodicity theorem, which reads in this case

$$S_1(E, \hat{\chi}_{C(\theta,\Delta\theta)}) = \frac{1}{N(E)} \sum_{E_n \le E} \left| \int_{C(\theta,\Delta\theta)} |\hat{\psi}_n(p)|^2 dp - \frac{\Delta\theta}{2\pi} \right| \to 0 \quad \text{for } E \to \infty. \qquad (59)$$

The results for $S_1(E, \hat{\chi}_{C(\theta_i,\Delta\theta)})$ are shown in Fig. 14 for the stadium billiard and in Fig. 15 for the cardioid billiard. In each case 2000 eigenfunctions have been used. For the cardioid billiard the inset shows a double-logarithmic representation together with the fits of $S_1^{\text{fit}}(E)$ [Eq. (49)]. For the cosine billiard no computations of the rate $S_1(E, \hat{\chi}_{C(\theta_i,\Delta\theta)})$ in momentum space have been performed.

As in position space one expects that the rate is strongly influenced by non-quantum-ergodic subsequences of eigenfunctions. For the bouncing-ball modes in the stadium billiard one has

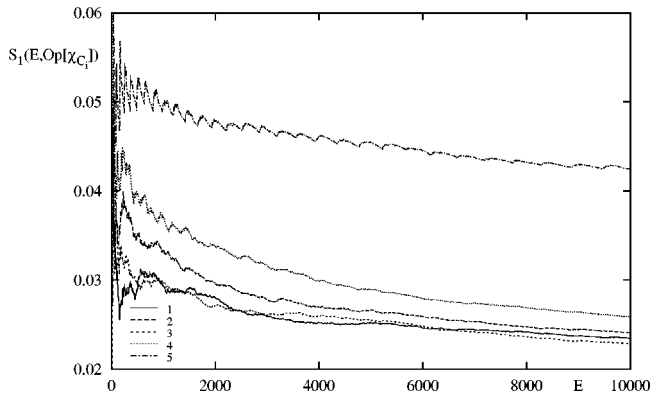

FIG. 14. Plot of $S_1(E, \hat{\chi}_{C(\theta_i,\Delta\theta)})$ for $\theta_i = (i-1/2)(\pi/10)$ with $i = 1,\ldots,5$ and $\Delta\theta = \pi/10$ for the stadium billiard using the first 2000 eigenfunctions.

$$\lim_{E_{n''}\to\infty} \int_{C(\theta,\Delta\theta)} |\hat{\psi}_{n''}(p)|^2 dp = \begin{cases} 0, & \text{for } \frac{\pi}{4} \notin]\theta - \Delta\theta, \theta + \Delta\theta[\\ 1 & \text{for } \frac{\pi}{4} \in]\theta - \Delta\theta, \theta + \Delta\theta[\end{cases} \qquad (60)$$

and so the coefficient $\nu''_{\text{BB}}(\hat{\chi}_{C(\theta_i,\Delta\theta)})$ in the model (43) for $S_1(E, \hat{\chi}_{C(\theta_i,\Delta\theta)})$ is given by

$$\nu''_{\text{BB}}(\hat{\chi}_{C(\theta_i,\Delta\theta)}) = \begin{cases} \frac{1}{20} & \text{for } i = 1,\ldots,4 \\ \frac{19}{20} & \text{for } i = 5. \end{cases} \qquad (61)$$

The results for the rate of quantum ergodicity, characterized by ε, are listed in Table V. It turns out that the rate is slower than the rate of quantum ergodicity for the small domains in configuration space. Moreover, the agreement of $S_1(E, \hat{\chi}_{C(\theta_i,\Delta\theta)})$ with the fit is not as good as in the case of $S_1(E, \chi_D)$; in particular the fluctuations of $S_1(E, \hat{\chi}_{C(\theta_i,\Delta\theta)})$ are much larger than in position space.

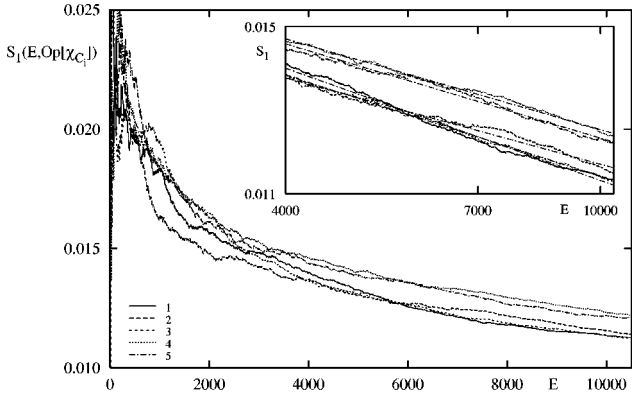

FIG. 15. Plot of $S_1(E, \hat{\chi}_{C(\theta_i,\Delta\theta)})$ for $\theta_i = (i-1/2)(\pi/10)$ with $i = 1,\ldots,5$ and $\Delta\theta = \pi/10$ for the cardioid billiard using the first 2000 eigenfunctions.

TABLE V. Rate of quantum ergodicity obtained from a fit of $S_1^{\mathrm{fit}}(E)=aE^{-1/4+\varepsilon}$ to the numerically obtained function $S_1(E,\hat{\chi}_{C(\theta_i,\Delta\theta)})$ for the different systems and angle sectors $C(\theta_i,\Delta\theta)$.

System	Domain	ε
stadium	1	0.15
	2	0.12
	3	0.15
	4	0.09
	5	0.18
cardioid	1	0.050
	2	0.075
	3	0.026
	4	0.079
	5	0.076

In the stadium billiard the interval 5, which corresponds the direction of the bouncing ball orbits, shows the slowest rate. However, as we already noted in the discussion of the rate in position space, the bouncing-ball modes alone cannot cause such a slow rate because their counting function increases only as $E^{3/4}$. So a considerable number of the additional non-quantum-ergodic states that are responsible for the slow rate in position space must also have an enhanced momentum density around $\pi/2$. However, the slow rates for the other angular intervals indicate that not all non-quantum-ergodic states show this behavior in momentum space.

For both billiards one observes that the order of magnitude of ε in momentum space is the same as for the large domains in position space. Therefore, the results are compatible with the results in position space, but the large fluctuations indicate that one has to go higher in the energy in momentum space than in position space.

C. Fluctuations of expectation values

Another aspect of great interest is how the expectation values $\langle\psi_n,\mathrm{A}\psi_n\rangle$ fluctuate around their mean value $\overline{\sigma(\mathrm{A})}$. Since the mean fluctuations decrease for large n, one has to consider the distribution of

$$\xi_n=\frac{\langle\psi_n,\mathrm{A}\psi_n\rangle-\overline{\sigma(\mathrm{A})}}{\sqrt{\widetilde{S}_2(E_n,\mathrm{A})}}. \tag{62}$$

Here $\widetilde{S}_2(E,\mathrm{A})=\Xi S_2(E,\mathrm{A})$, with Ξ being a correction necessary to ensure that the distribution of ξ_n has unit variance; see below for an explanation. So the question is whether a limit distribution $P(\xi)$ of ξ_n exists in the weak sense, i.e.,

$$\lim_{N\to\infty}\frac{1}{N}\sum_{n=1}^{N}g(\xi_n)=\int_{-\infty}^{\infty}g(\xi)P(\xi)d\xi, \tag{63}$$

where $g(\xi)$ is a bounded continuous function. It is natural to conjecture that this distribution tends to a Gaussian normal distribution

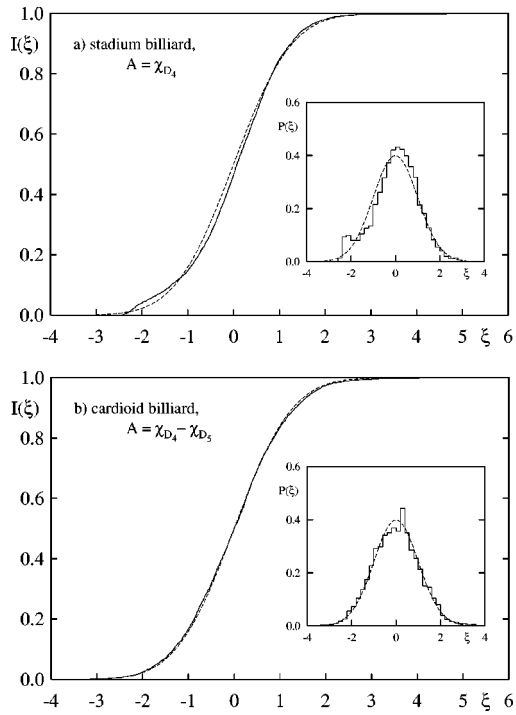

FIG. 16. Cumulative distribution of $\xi_n=[\langle\psi_n,A\psi_n\rangle-\overline{\sigma(A)}]/\sqrt{\widetilde{S}_2(E_n,A)}$ for the stadium billiard for domain 4, $A=\chi_{D_4}$, and for the cardioid billiard with observable $A=\chi_{D_4}-\chi_{D_5}$. In both cases we haven chosen $n\in[2000,6000]$. The dashed curve corresponds to the cumulative normal distribution. The insets show the distribution of ξ_n together with the normal distribution with zero mean and unit variance [Eq. (64)] (dashed curve).

$$P(\xi)=\frac{1}{\sqrt{2\pi}}\exp(-\xi^2/2), \tag{64}$$

as in random matrix theory (see [44], Sec. VII). Note that this is a conjecture for every observable, i.e., the asymptotic distribution should be independent of the special observable under investigation. For hyperbolic surfaces a study of $P(\xi)$ for an observable in position space is contained in [17], where good agreement with a Gaussian normal distribution was observed. In [16] $P(\xi)$ was studied for the Baker map and the hydrogen atom in a strong magnetic field and fair agreement with a Gaussian was found.

However, already from the plots of $d_i(n)$ shown in Fig. 3 it is clear that the fluctuations are not symmetrically distributed around zero, but have more peaks with large positive values. The reason is that $d_i(n)=\langle\psi_n,\chi_{D_i}\psi_n\rangle-V(D_i)/V(\Omega)$ has to satisfy the inequality

$$-\frac{V(D_i)}{V(\Omega)}\leqslant\langle\psi_n,\chi_{D_i}\psi_n\rangle-\frac{V(D_i)}{V(\Omega)}\leqslant 1-\frac{V(D_i)}{V(\Omega)}. \tag{65}$$

This already indicates that the approach to an asymptotic Gaussian behavior could be rather slow. Therefore, we have tested additionally for the cardioid billiard the observable $A=\chi_{D_4}-\chi_{D_5}$ where the expectation values fluctuate symmetrically around zero and one expects a faster approach to a Gaussian behavior. In Fig. 16(a) we show the cumulative distribution

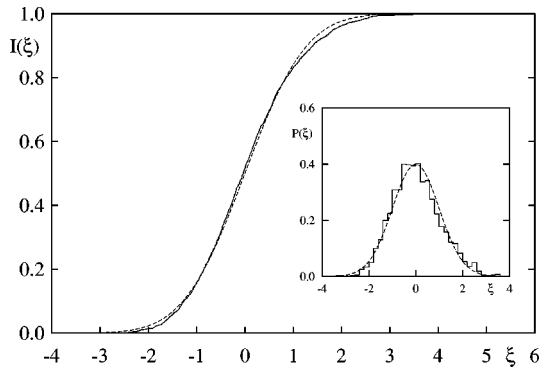

FIG. 17. Cumulative distribution of $\xi_n=[\langle\psi_n,A\psi_n\rangle-\overline{\sigma(A)}]/\sqrt{\widetilde{S}_2(E_n,A)}$ for the cardioid billiard, for the observable $\chi_{C(\theta,\Delta\theta)}(p)$ in momentum space with $\theta=5\pi/20$ and $\Delta\theta=\pi/10$. The dashed curve corresponds to the cumulative normal distribution. The inset shows the distribution of ξ_n together with the normal distribution with zero mean and unit variance [Eq. (64)] (dashed curve).

$$I_N(\xi)=\frac{1}{N}\sum_{\xi_n<\xi}1 \tag{66}$$

for domain D_4 of the stadium billiard and in Fig. 16(b) $I_N(\xi)$ is shown for the observable $A=\chi_{D_4}-\chi_{D_5}$ in case of the cardioid billiard. In both cases all values of ξ_n with $n\in[2000,6000]$ have been taken into account, giving $N=4000$. For the rate $S_2(E,\chi_D)$ we used the result of a fit to $S_2^{\rm fit}(E)=aE^{\alpha}$. The insets show the corresponding distributions of ξ_n in comparison with the normal distribution [Eq. (64)]. Notice that no further fit of the mean or the variance of the Gaussian has been made. Figure 16(a) is the case for which we have found the worst agreement with a Gaussian (of all the small domains we have tested). The observable chosen for Fig. 16(b) gives very good agreement with the Gaussian distribution. In the case of χ_{D_4} in the stadium billiard there is a significant peak around $\xi=-2$, which is due to the bouncing-ball modes, for which $\langle\psi_{n''},\chi_{D_4}\psi_{n''}\rangle$ is approximately zero; see Fig. 3. Therefore, one has a larger fraction with negative $\xi_{n''}$. For the distribution in case of the observable $A=\chi_{D_4}-\chi_{D_5}$ of the cardioid billiard we obtain a significance level of 23% for the Kolmogorov-Smirnov test (see, e.g., [72]) with respect to the cumulative normal distribution.

We also studied the distribution of ξ_n for the observables $a(p,q)=a(p)=\chi_{C(\theta,\Delta\theta)}(p)$ in momentum space. For the stadium billiard the computed distributions show in the considered energy range clear deviations from a Gaussian, as one already expects from Fig. 14. The best result was obtained for the cardioid billiard for the interval given by $i=3$ [with $\theta_i=(i-1/2)(\pi/10)$ and $\Delta\theta=(\pi/10)$] and is shown in Fig. 17. The agreement is quite good; the Kolmogorov-Smirnow test gives a significant level of 29%.

There is one subtle point concerning the variance of the distribution of ξ_n. Since $S_2(E,A)$ does not represent a local variance around E, but a global one, it is necessary to take this into account to obtain for the fluctuations a variance of unity. If the rate behaves as $S_2(E,A)=aE^{\alpha}$, then the correction Ξ is given by $\Xi=\alpha+1$, e.g., for $\alpha=-1/2$ we have $\Xi=1/2$. See [63] for a more detailed discussion on this point in the case of the distribution of the normalized mode fluctuations.

Let us now discuss the influence of non-quantum-ergodic sequences to the possible limit distribution. Assume that the rate for the quantum-ergodic states is $S_2'(E,A)\sim aE^{-\alpha}$ with some power α. If we have a subsequence of non-quantum-ergodic states such that the total rate is $S_2(E,A)\sim a'E^{-\alpha'}$, we can have two different situations, either $\alpha=\alpha'$ or $\alpha<\alpha'$. In the first case the non-quantum-ergodic states have no influence on the limit distribution. In the second case where the non-quantum-ergodic states dominate the rate, the normalization by a rate that is slower than the one of the quantum-ergodic subsequence implies that we have $P(\xi)=\delta(\xi)$.

If one instead normalizes the fluctuations with the rate of the quantum-ergodic subsequence $S_2'(E,A)$,

$$\widetilde{\xi}_n:=\frac{\langle\psi_n,A\psi_n\rangle-\overline{\sigma(A)}}{\sqrt{\widetilde{S}_2'(E_n,A)}}, \tag{67}$$

with $\widetilde{S}_2'(E_n,A)=\Xi S_2'(E,A)$, then the limit distribution is determined only by the quantum-ergodic subsequence, independently of the behavior of the non-quantum-ergodic subsequence. To see this we split Eq. (63) into the different parts

$$\frac{1}{N(E)}\sum_{E_n\leqslant E}g(\widetilde{\xi}_n)=\frac{N'(E)}{N(E)}\frac{1}{N'(E)}\sum_{E_{n'}\leqslant E}g(\widetilde{\xi}_{n'})+\frac{N''(E)}{N(E)}\frac{1}{N''(E)}\sum_{E_{n''}\leqslant E}g(\widetilde{\xi}_{n''}). \tag{68}$$

Since $\lim_{E\to\infty}N'(E)/N(E)=1$, $\lim_{E\to\infty}N''(E)/N(E)=0$, and $1/N''(E)\Sigma_{E_{n''}\leqslant E}g(\widetilde{\xi}_{n''})\leqslant\max_{\xi\in\mathbf{R}}g(\xi)$, one gets

$$\lim_{E\to\infty}\frac{1}{N(E)}\sum_{E_n\leqslant E}g(\widetilde{\xi}_n)=\lim_{E\to\infty}\frac{1}{N'(E)}\sum_{E_{n'}\leqslant E}g(\widetilde{\xi}_{n'}). \tag{69}$$

We conjecture that the fluctuations of the quantum-ergodic subsequence is Gaussian and therefore all fluctuations, when normalized with the rate of the quantum-ergodic subsequence, are Gaussian.

IV. SUMMARY

The aim of the present paper is to give a detailed study of the rate of quantum ergodicity in Euclidean billiards. We first have given a short introduction to the quantum ergodicity theorems in terms of pseudodifferential operators. We have shown that the quantum ergodicity theorems of Shnirelman, Zelditch, Colin de Verdiére, and others are equivalent to a weak form of the semiclassical eigenfunction hypothesis for ergodic systems put forth in [9–12]. That is, the quantum ergodicity theorem is equivalent to the statement that for ergodic systems the Wigner functions $W_n(p,q)$ fulfill

$$W_{n_j}(p,q) \sim \frac{1}{V(\Sigma_{E_{n_j}})}\,\delta(H(p,q)-E_{n_j}) \tag{70}$$

for $E_{n_j}\to\infty$ and $\{n_j\}\subset\mathbf{N}$ a subsequence of density one.

Of great importance for the practical applicability of the quantum ergodicity theorem is the question at which rate quantum-mechanical expectation values $\langle\psi_n, A\psi_n\rangle$ tend to their mean value $\overline{\sigma(A)}$. Different arguments were presented previously in favor of an expected rate of quantum ergodicity $S_1(E,\mathrm{A})=O(E^{-1/4+\varepsilon})$ for all $\varepsilon>0$, in the case of strongly chaotic systems. In Sec. II D we discussed the influence of non-quantum-ergodic subsequences to the rate. If their counting function increases sufficiently fast, they can dominate the behavior of $S_1(E,\mathrm{A})$ asymptotically. Together with results from [46] for the number of bouncing-ball modes in certain billiards, it follows that one can find for arbitrary $\delta>0$ an ergodic billiard for which $S_1(E,\mathrm{A})=O(E^{-\delta})$. That is, the quantum ergodicity theorem gives a sharp bound, which cannot be improved without additional assumptions on the system.

We furthermore developed a simple model for the behavior of $S_1(E,A)$ in the presence of non-quantum-ergodic eigenfunctions, whose main ingredient is that the quantum-ergodic eigenfunctions should obey the optimal rate $E^{-1/4}$. The discussion shows that the total rate of quantum ergodicity can be strongly influenced by those exceptional subsequences. Not only can they cause the rate to be much slower than $E^{-1/4}$, they can lead as well to a grossly different behavior of $S_1(E,A)$ at low, intermediate, and high energies.

The numerical investigations are carried out for three types of Euclidean billiards: the stadium billiard (with different parameters), the cosine billiard, and the cardioid billiard. The results are based on 2000 eigenfunctions for the cosine billiard and up to 6000 eigenfunctions for the stadium and the cardioid billiard. As observables we have used characteristic functions of different domains in position space and also a class of observables in momentum space.

It turns out that the rate of quantum ergodicity in position space is in good agreement with a power-law decay $S_1(E,A)\sim E^{-1/4+\varepsilon}$. The difference ε between the exponent and 1/4 is found to be small for several domains and systems. However, we also find a number of significant examples showing a slow rate (i.e., $\varepsilon>0$ and not small). These are discussed in detail and can be attributed to subsequences of localized eigenfunctions.

For the cosine billiard we find that the rate agrees well with the expected rate, in particular for the small domains. However, asymptotically the rate has to obey $S_1(E,A)\sim E^{-1/10}$ because the counting function of the bouncing-ball modes increases as $E^{9/10}$. The asymptotic regime for the rate lies far beyond any presently computable number of energy levels. By incorporating the knowledge of the counting function obtained from our previous work, we tested our model (43) for the rate for all the considered domains.

For the stadium billiard the situation is more complicated: Here the counting function of the bouncing-ball modes increases as $E^{3/4}$ and therefore, as discussed in Sec. II D, cannot influence the rate. However, we find for the stadium billiard that the rate is for several domains in position space much slower than expected. After discussing and testing several possibilities, our explanation for this observation is that in the stadium billiard there exists a much larger subsequence of eigenfunctions that have an enhanced probability density in the rectangular part of the billiard than just the bouncing-ball modes. They nevertheless have density zero, but their counting function increases more strongly than $E^{3/4}$. Of course, we cannot decide whether this subsequence either has a quantum limit different from the Liouville measure, or if it is a quantum-ergodic subsequence with an exceptionally slow rate.

For the cardioid billiard we also have domains for which the rate is proportional to $E^{-1/4}$. However, we also find significant exceptions; in particular for domain D_3 the rate is much slower, and this can be attributed to a number of eigenstates that show localization along the unstable periodic orbit $\overline{AB}$. For the cardioid billiard we also tested the result from [16] [Eq. (33)] for the domains D_4 and D_5, for which the rate is closest to the optimal rate. However, the semiclassical result does not agree with our numerical results for the rate. It would be interesting to study this in more detail.

From our numerical results we obtain the following general picture: In the studied systems there is a quantum-ergodic subsequence of density one whose rate is $S_1'(E,\mathrm{A})=O(E^{-1/4+\varepsilon})$. If one observes a slower rate of $S_1(E,A)$ by using all eigenfunctions, this is caused by a subsequence of density zero, whose counting function increases more strongly than $E^{3/4}$. These exceptional eigenfunctions show localization effects and probably they tend to some non-quantum-ergodic limit. However, we cannot rule out the possibility that they are quantum ergodic but with a much slower rate than the majority of eigenfunctions.

Furthermore, we have found an effect due to the boundary conditions. For domains lying next to the boundary we observed that the rate may be considerably faster at low energies. The qualitative explanation of the phenomenon is that the probability density of the eigenstates shows enhanced fluctuations near the boundary because of the boundary conditions.

Using an observable depending only on the momentum, we studied quantum ergodicity in momentum space too. We find that, in general, the rate of quantum ergodicity is of the same magnitude as for the large domains in position space. Furthermore, the oscillations of $S_1(E,A)$ are larger in momentum space, which might indicate that one has to go higher in the energy in momentum space than in position space.

We also studied the distribution of the suitably normalized fluctuations of $\langle\psi_n, A\psi_n\rangle-\overline{\sigma(A)}$ [see Eq. (62)] for operators both in position space and in momentum space. For the observable $A=\chi_{D_4}-\chi_{D_5}$, in the case of the cardioid billiard we find very good agreement with a Gaussian normal distribution and in the case of observables depending only on the momentum good agreement is found. However, for the stadium billiard (and also domain D_3 for the cardioid billiard) we clearly find that again subsequences of non-quantum-ergodic states may have a considerable influence. If they dominate $S_2(E,A)$, the distribution will tend to a δ function due to the normalization by $\sqrt{S_2(E,A)}$. However, when normalizing instead with the rate of the quantum-ergodic states $\widetilde{S}_2'(E,\mathrm{A})$, we expect a universal Gaussian distribution of the fluctuations.

As possible investigations for the future it seems very interesting to study whether the expression given in [16] for the rate in terms of the classical correlation function can describe our numerical results. In particular, for the cardioid billiard a more detailed investigation along these lines seems promising as this system is the most generic one of the three studied systems and we find both the optimal rate and also clear deviations. The present paper also shows that a detailed understanding of the phenomenon of scarred eigenfunctions is necessary because these clearly affect the rate of quantum ergodicity.

ACKNOWLEDGMENTS

We would like to thank Dr. R. Aurich, Dr. J. Bolte, T. Hesse, Dr. M. Sieber, and Dr. F. Steiner for useful discussions and comments. Furthermore, we are grateful to Dr. M. Robnik and Dr. T. Prosen for the kind provision of the eigenvalues of the cardioid billiard. Figure 13(a) has been visualized using GEOMVIEW from The Geometry Center of the University of Minnesota and then rendered using BLUE MOON RENDERING TOOLS written by L. I. Gritz. A.B. acknowledges support by the Deutsche Forschungsgemeinschaft under Contract No. DFG-Ste 241/7-2.

APPENDIX A: KOHN-NIRENBERG QUANTIZATION

In the mathematical literature one often prefers a different quantization procedure, sometimes called the Kohn-Nirenberg quantization [20,21], and the literature on quantum ergodicity often refers to this quantization procedure. With the symbol $a \in S^m(\mathbf{R}^2 \times \Omega)$ one associates the operator

$$\hat{a}^{\mathrm{KN}} f(q) := \frac{1}{(2\pi)^2} \int_{\mathbf{R}^2} e^{ipq} a(p,q) \hat{f}(p) dp, \qquad \text{(A1)}$$

where $\hat{f}(p) := \int_\Omega e^{-iqp} f(q) dq$ is the Fourier transform of f. The principal symbol is defined in the same way as before, i.e., if $a \sim \Sigma_{k=0}^{\infty} a_{m-k}$, then the leading term a_m is called the principal symbol, $\sigma^{\mathrm{KN}}(\hat{a}^{\mathrm{KN}}) = a_m$.

The usual quantum ergodicity theorem is now the same theorem as we have stated it, but with the Kohn-Nirenberg principal symbol σ^{KN} instead of the principal symbol corresponding to the Weyl symbol that we have used. However, it is well known (see [21,20]) that if $a \in S^m(\mathbf{R}^n \times \mathbf{R}^n)$, then the Weyl symbol of the Kohn-Nirenberg operator belongs to the same symbol space $W[\hat{a}^{\mathrm{KN}}] \in S^m(\mathbf{R}^n \times \mathbf{R}^n)$ and that the principal symbol coincides with the Kohn-Nirenberg principal symbol

$$\sigma(\hat{a}^{\mathrm{KN}}) = \sigma^{\mathrm{KN}}(\hat{a}^{\mathrm{KN}}). \qquad \text{(A2)}$$

Therefore, the two formulations of the quantum ergodicity theorem are equivalent.

APPENDIX B: GENERALIZATIONS OF THE QUANTUM ERGODICITY THEOREM

Assume we have given a quantum limit μ_k on Σ_1, that is, we have a subsequence of eigenfunctions $\{\psi_{n_j}\}_{j \in \mathbf{N}}$, such that

$$\lim_{j \to \infty} \langle \psi_{n_j}, A \psi_{n_j} \rangle = \int_{\Sigma_1} \mu_k(p,q) \sigma(A)(p,q) d\mu \qquad \text{(B1)}$$

for all $A \in S^0_{\mathrm{cl}}(\Omega)$. We want to discuss the lift of μ_k from Σ_1 to the whole phase space.

To this end we express the expectation values for an operator of arbitrary order $m \in \mathbf{R}$ by the expectation values of an operator of order zero. This can be achieved by using the fact that for every $m \in \mathbf{R}$, $(-\Delta)^{m/2}$ is a pseudodifferential operator of order m with principal symbol $\sigma[(-\Delta)^{m/2}] = [\sigma(-\Delta)]^{m/2} = H(p,q)^{m/2}$; see [25,26,22]. By multiplying an operator $A \in S^m(\mathbf{R}^m)$ of order m by operator $(-\Delta)^{-m/2}$, which is of order $-m$, we get an operator $(-\Delta)^{-m/2} A \in S^0(\mathbf{R}^n)$ of order zero. For the expectation values of A we therefore have

$$\langle \psi_{n_j}, A \psi_{n_j} \rangle = E_{n_j}^{m/2} \left\langle \psi_{n_j}, (-\Delta)^{-m/2} A \psi_{n_j} \right\rangle \qquad \text{(B2)}$$

and on the right-hand side we have an operator of order zero.

The principal symbol of $(-\Delta)^{-m/2} A$ is, according to Eq. (11), given by $\sigma[(-\Delta)^{-m/2}] \sigma(A) = H(p,q)^{-m/2} \sigma(A)$ and since by definition $H(p,q) = 1$ on Σ_1, we obtain from Eqs. (B1) and (B2)

$$\lim_{j \to \infty} E_{n_j}^{-m/2} \langle \psi_{n_j}, A \psi_{n_j} \rangle = \int_{\Sigma_1} \mu_k(p,q) \sigma(A)(p,q) d\mu. \qquad \text{(B3)}$$

Thus Eq. (B3) provides the extension of the quantum ergodicity theorem to pseudodifferential operators of arbitrary order m.

APPENDIX C: CONNECTION TO THE SEMICLASSICAL EIGENFUNCTION HYPOTHESIS

By introducing the definition of the Liouville measure μ, Eq. (B3) can be written as

$$\langle \psi_{n_j}, A \psi_{n_j} \rangle \sim E_{n_j}^{m/2} \int \int \mu_k(p,q) \sigma(A)(p,q) \times \frac{\delta(H(p,q)-1)}{V(\Sigma_1)} dp\, dq. \qquad \text{(C1)}$$

If one uses the homogeneity of $\sigma(A)$, i.e., $E_{n_j}^{m/2} \sigma(A)(p,q) = \sigma(A)(E_{n_j}^{1/2} p, q)$, and performs a change of the momentum coordinates from p to $E_{n_j}^{-1/2} p$ one obtains

$$\begin{aligned} \langle \psi_{n_j}, A \psi_{n_j} \rangle &\sim \int \int \mu_k(E_{n_j}^{-1/2} p, q) \sigma(A)(p,q) \times \frac{\delta(H(E_{n_j}^{-1/2} p, q) - 1)}{V(\Sigma_1)} E_{n_j}^{-n/2} dp\, dq \\ &= \int \int \mu_k(E_{n_j}^{-1/2} p, q) \sigma(A)(p,q) \times \frac{\delta(H(p,q) - E_{n_j})}{V(\Sigma_1) E_{n_j}^{n/2-1}} dp\, dq, \end{aligned} \qquad \text{(C2)}$$

where furthermore the homogeneity properties of $H(p,q)$

and of the δ function have been used. In terms of the Wigner functions W_{n_j} corresponding to ψ_{n_j}, Eq. (C2) reads

$$\int\int \sigma(A)(p,q)W_{n_j}(p,q)dp\,dq \sim \int\int \sigma(A)(p,q)\mu_k(E_{n_j}^{-1/2}p,q) \times \frac{\delta(H(p,q)-E_{n_j})}{V(\Sigma_1)E_{n_j}^{n/2-1}}dp\,dq, \tag{C3}$$

where $\sigma(A)(p,q)$ can be any function homogeneous in p of degree m, for some arbitrary $m \in \mathbf{R}$. However, since the set of all polynomials in p is already dense in $C^\infty(\mathbf{R}^2\times\Omega)$ the set of homogeneous functions in p is dense in $C^\infty(\mathbf{R}^2\times\Omega)$ too. Therefore, one gets

$$W_{n_j}(p,q) \sim \mu_k(E_{n_j}^{-1/2}p,q)\,\frac{\delta(H(p,q)-E_{n_j})}{V(\Sigma_1)E_{n_j}^{n/2-1}}. \tag{C4}$$

Note that $V(\Sigma_1)E_{n_j}^{n/2-1}=V(\Sigma_{E_{n_j}})$ and if we extend $\mu_k(p,q)$ from Σ_1 to the whole phase space by requiring it to be homogeneous of degree zero, $\mu_k(p,q):=\mu_k(p/\sqrt{H(p,q)},q)$ for $(p,q)\notin\Sigma_1$, then we finally can write

$$W_{n_j}(p,q) \sim \mu_k(p,q)\,\frac{\delta(H(p,q)-E_{n_j})}{V(\Sigma_{E_{n_j}})} \quad \text{for } j\to\infty \tag{C5}$$

for a subsequence $\{n_j\}\subset\mathbf{N}$ of density one. This shows that the quantum ergodicity theorem is equivalent to the semiclassical eigenfunction hypothesis for ergodic systems for a subsequence of density one.

[1] A. I. Shnirelman, Usp. Mat. Nauk **29**, 181 (1974).
[2] A. I. Shnirelman, in *KAM Theory and Semiclassical Approximations to Eigenfunctions*, edited by V. F. Lazutkin (Springer, Berlin, 1993).
[3] S. Zelditch, Duke Math. J. **55**, 919 (1987).
[4] Y. Colin de Verdière, Commun. Math. Phys. **102**, 111 (1985).
[5] B. Helffer, A. Martinez, and D. Robert, Commun. Math. Phys. **109**, 313 (1987).
[6] P. Sarnak, Isr. Math. Conf. Proc. **8**, 183 (1995).
[7] A. Knauf and Ya. G. Sinai, *Classical Nonintegrability, Quantum Chaos* (Birkäuser, Basel 1997), DMV-Seminar 27.
[8] E. P. Wigner, Phys. Rev. **40**, 749 (1932).
[9] A. Voros, Ann. Inst. Henri Poincaré, Sect. A **24**, 31 (1976).
[10] A. Voros, Ann. Inst. Henri Poincaré, Sect. A **26**, 343 (1977).
[11] M. V. Berry, J. Phys. A **10**, 2083 (1977).
[12] M. V. Berry, in *Comportement Chaotique des Systèmes Déterministes—Chaotic Behaviour of Deterministic Systems*, edited by G. Ioss, R. H. G. Hellemann, and R. Stora (North-Holland, Amsterdam, 1983), pp. 171–271.
[13] S. Zelditch, Commun. Math. Phys. **160**, 81 (1994).
[14] S. Zelditch, Commun. Partial Diff. Eq. **19**, 1565 (1994).
[15] W. Luo and P. Sarnak, Publ. Math., Inst. Hautes Etud. Sci. **81**, 207 (1995).
[16] B. Eckhardt, S. Fishman, J. Keating, O. Agam, J. Main, and K. Müller, Phys. Rev. E **52**, 5893 (1995).
[17] R. Aurich and M. Taglieber, Ulm Report No. ULM-TP/97-6, chao-dyn/9707016.
[18] E. J. Heller, Phys. Rev. Lett. **53**, 1515 (1984).
[19] S. W. McDonald and A. N. Kaufmann, Phys. Rev. A **37**, 3067 (1988).
[20] L. Hörmander, *The Analysis of Linear Partial Differential Operators III* (Springer, Berlin, 1985).
[21] G. B. Folland, *Harmonic Analysis in Phase Space*, Annals of Mathematics Studies Vol. 12 (Princeton University Press, Princeton, 1989).
[22] M. E. Taylor, *Pseudodifferential Operators*, Princeton Mathematical Series No. 34 (Princeton University Press, Princeton, 1981).
[23] R. Schubert, Diploma thesis, II. Institut für Theoretische Physik, Universität Hamburg, 1996 (unpublished).
[24] L. Hörmander, *The Analysis of Linear Partial Differential Operators I* (Springer, Berlin, 1983).
[25] R. T. Seeley, Proc. Symp. Pure Math. **10**, 288 (1967).
[26] R. T. Seeley, Am. J. Math. **91**, 889 (1969).
[27] L. Hörmander, *The Analysis of Linear Partial Differential Operators IV* (Springer, Berlin, 1985).
[28] D. Robert, *Autour de l'Approximation Semi-Classique* (Birkhäuser, Boston, 1987).
[29] S. Zelditch, J. Funct. Anal. **94**, 415 (1990).
[30] S. Zelditch and M. Zworski, Commun. Math. Phys. **175**, 673 (1996).
[31] P. Gérard and E. Leichtnam, Duke Math. J. **71**, 559 (1993).
[32] D. Jakobson, Ann. Math. **145**, 235 (1997).
[33] S. Zelditch, Commun. Math. Phys. **146**, 61 (1992).
[34] D. Jakobson and S. Zelditch (unpublished).
[35] P. Walters, *An Introduction to Ergodic Theory* (Springer-Verlag, Berlin, 1982).
[36] D. Jakobson, Ann. Inst. Fourier **44**, 1477 (1994).
[37] D. Jakobson, Ann. Inst. Fourier **47**, 967 (1997).
[38] L. A. Bunimovich, Funct. Anal. Appl. **8**, 254 (1974).
[39] Ya. G. Sinai, Russ. Math. Surv. **25**, 137 (1970).
[40] L. A. Bunimovich, Zh. Éksp. Teor. Fiz. **89**, 1452 (1985) [Sov. Phys. JETP **62**, 842 (1985)].
[41] P. Dahlqvist and R. Artuso, Phys. Lett. A **219**, 212 (1996).
[42] M. Srednicki, Phys. Rev. E **50**, 888 (1994).
[43] M. Srednicki and F. Stiernelof, J. Phys. A **29**, 5817 (1996).
[44] T. A. Brody, J. Flores, J. B. French, P. A. Mello, A. Pandey, and S. S. M. Wong, Rev. Mod. Phys. **53**, 385 (1981).
[45] S. W. McDonald and A. N. Kaufmann, Phys. Rev. Lett. **42**, 1189 (1979).
[46] A. Bäcker, R. Schubert, and P. Stifter, J. Phys. A **30**, 6783 (1997).
[47] L. A. Bunimovich, Commun. Math. Phys. **65**, 295 (1979).
[48] B. Li, Phys. Rev. E **55**, 5376 (1997).
[49] F. P. Simonotti, E. Vergini, and M. Saraceno, Phys. Rev. E **56**, 3859 (1997).

[50] P. Stifter, Diploma thesis, Abteilung für Quantenphysik, Universität Ulm, 1993 (unpublished).
[51] P. Stifter, Ph.D. thesis, Abteilung für Quantenphysik, Universität Ulm, 1996, (unpublished).
[52] M. Robnik, J. Phys. A **16**, 3971 (1983).
[53] M. Wojtkowski, Commun. Math. Phys. **105**, 391 (1986).
[54] D. Szász, Commun. Math. Phys. **145**, 595 (1992).
[55] R. Markarian, Nonlinearity **6**, 819 (1993).
[56] C. Liverani and M. P. Wojtkowski, in *Dynamics Reported. Expositions in Dynamical Systems*, edited by C. K. R. T. Jones, U. Kirchgraber, and H. O. Walther, Landolt-Börnstein, New Series, Vol. 4 (Springer-Verlag, Berlin, 1995), pp. 130–202.
[57] N. I. Chernov and C. Haskell, Ergodic Theory Dynamical Syst. **16**, 19 (1996).
[58] H. Bruus and N. D. Whelan, Nonlinearity **9**, 1023 (1996).
[59] A. Bäcker and H. R. Dullin, J. Phys. A **30**, 1991 (1997).
[60] A. Bäcker and N. Chernov, Nonlinearity **11**, 79 (1998).
[61] M. Robnik, J. Phys. A **17**, 1049 (1984).
[62] A. Bäcker, F. Steiner, and P. Stifter, Phys. Rev. E **52**, 2463 (1995).
[63] R. Aurich, A. Bäcker, and F. Steiner, Int. J. Mod. Phys. B **11**, 805 (1997).
[64] T. Prosen and M. Robnik (private communication).
[65] M. V. Berry and M. Robnik, J. Phys. A **19**, 649 (1986).
[66] T. Prosen and M. Robnik, J. Phys. A **26**, 2371 (1993).
[67] R. J. Riddel, Jr., J. Comput. Phys. **31**, 21 (1979).
[68] M. V. Berry and M. Wilkinson, Proc. R. Soc. London, Ser. A **392**, 15 (1984).
[69] R. Aurich and F. Steiner, Physica D **64**, 185 (1993).
[70] G. Tanner, J. Phys. A **30**, 2863 (1997).
[71] M. Sieber and F. Steiner, Phys. Lett. A **148**, 415 (1990).
[72] W. H. Press, S. A. Teukolsky, W. T. Vetterling, and B. P. Flannery, *Numerical Recipes in C. The Art of Scientific Computing*, 2nd ed. (Cambridge University Press, Cambridge, 1992).